8-3-2018

Strain Variation in Low-grade Metamorphic Thrust Sheets: An Example from the Northern Taconic Allochthon of Vermont and New York, USA

Jessica Robinson
jessica.robinson@uconn.edu

Strain Variation in Low-grade Metamorphic Thrust Sheets: An Example from the Northern Taconic Allochthon of Vermont and New York, USA

Jessica Marie Robinson

B.S. Geology, University of the Pacific, 2016

A Thesis

Submitted in Partial Fulfillment of the

Requirements for the Degree of

Master of Science

At the

University of Connecticut

2018

APPROVAL PAGE

Masters of Science Thesis

Strain Variation in Low-grade Metamorphic Thrust Sheets: An Example from the Northern Taconic Allochthon of Vermont and New York, USA

Presented by

Jessica Marie Robinson, B.S.

Major Advisor_____

Jean M. Crespi

Associate Advisor_____

Julie C. Fosdick

Associate Advisor_____

Timothy B. Byrne

University of Connecticut

2018

Acknowledgments

Thank you to my advisor, Dr. Jean Crespi. Your continuous guidance and support has helped me both grow as a research scientist and develop the confidence that I can succeed in the geosciences. Working with you in the lab and in the field has been genuinely enjoyable and I'm grateful that you were my advisor.

Thank you to my committee members, Dr. Julie Fosdick and Dr. Tim Byrne. Your discussion, ideas, and feedback on my thesis has been invaluable.

Thank you to my fellow grad students. You have made living in Connecticut feel more like home and I am grateful for everything, fun times and stressful times, that we got to share. In particular, thank you to Jennifer Cooper-Bommels for being an excellent labmate and for the considerable assistance in the field.

I also want to thank the Center for Integrative Geosciences and the Geological Society of America for the financial support that made my thesis research possible.

Finally, thank you to my family for your encouragement and support of my education. Special thanks to my mom, Sarah. Whether I needed a shoulder to cry on, someone to rant to, or a swift kick in the seat to get going, you have always been there for me.

Table of Contents

List of Figures

List of Tables

Abstract

Thrust sheet emplacement is typically accompanied by internal deformation that can vary depending on a range of factors. In the Taconic slate belt in the northern part of the Giddings Brook thrust sheet of the Taconic allochthon, map-view curves and an along-strike change in structural level expose variations in internal deformation of a low-grade metamorphic thrust sheet. We characterized internal deformation during slaty cleavage formation by determining the orientations of cleavage and stretching lineation and by quantifying the strain using syntectonic fibers formed on subspherical core objects. The slate belt is everywhere characterized by top-to-west-northwest noncoaxial flow. The southern and northern domains have a north-northeast-striking, shallowly to moderately dipping slaty cleavage with a downdip stretching lineation. The strain magnitude and degree of fiber asymmetry, however, are lower in the structurally higher southern domain. The central domain has a north-northwest-striking, moderately dipping slaty cleavage with a moderately raking stretching lineation. A component of sinistral shear sets it apart from the other two domains, with the strain magnitude and degree of fiber asymmetry otherwise similar to the southern domain. We interpret the southern and northern domains as being dominated by dip-slip thrusting with strain increasing toward the base of the thrust sheet and the central domain as a region of inclined transpression. Two-dimensional kinematic models of thrust sheet deformation show that the southern and northern domains can be described by simple shear (with small amounts of thrust sheet thinning in the southern domain) in contrast to unmetamorphosed to weakly metamorphosed thrust sheets that exhibit thrust sheet thickening and higher-grade metamorphic thrust sheets that exhibit thrust sheet thinning. In addition, the dip-slip character

of the southern and northern domains combined with the lack of evidence for orogen-scale kinematic partitioning implies nearly orthogonal plate convergence during the Taconic orogeny in the northeastern United States.

Introduction

Thrust sheets deform internally through a combination of folding, faulting, and/or penetrative strain. This internal deformation has been evaluated using two-dimensional kinematic models involving some combination of simple shear, pure shear, and/or volume change (Ramsay, 1980; Coward and Kim, 1981; Kligfield et al., 1981; Sanderson, 1982; Coward and Potts, 1983; Fossen and Tikoff, 1993; Tikoff and Fossen, 1993). These models make predictions about the relation between the strain magnitude and the angle between the long axis of the strain ellipsoid and the base of the thrust sheet. Angles larger than predicted by simple shear alone imply thrust sheet thickening, and angles smaller than predicted by simple shear alone imply thrust sheet thinning. The models can also be used to understand the factors controlling heterogeneities in flow and strain magnitude. Their application improves estimates of total shortening, restorations of cross sections, and interpretations of thrust-belt evolution (Kligfield et al., 1981; Yonkee, 2005; Long et al., 2011).

Where thrust sheet thickening has been inferred, the strata are typically relatively competent and/or unmetamorphosed to weakly metamorphosed (e.g., Coward and Kim, 1981; Mitra, 1994; Yonkee, 2005; Weil and Yonkee, 2012; Nabavi et al., 2017). Weak lithologies and/or more highly metamorphosed strata, in contrast, are associated with thrust sheet thinning (e.g., Kligfield et al., 1981; Sanderson, 1982; Yonkee, 2005; Long et al., 2011). These observations led Long et al. (2011) to propose that the transition between these two modes of internal deformation occurs at the minimum temperature for quartz plasticity (~250–300 °C). The internal deformation of thrust sheets composed of slate-dominated stratigraphic successions, however, has received little attention in the context of kinematic models

illustrating the relative contributions of simple shear, pure shear, and volume change. This represents a gap in our understanding of the transition from external to internal thrust sheets.

The Taconic allochthon, which lies in the northeastern United States, was emplaced to the west onto approximately coeval strata of the Laurentian margin in a retoarc setting during the final stage of the Early to Late Ordovician Taconic orogeny (Macdonald et al., 2014, 2017; Karabinos et al., 2017). The Taconic slate belt lies in the northern part of the Giddings Brook thrust sheet, the largest and westernmost thrust sheet in the Taconic allochthon (Zen, 1967). In this area, different structural levels of the thrust sheet are exposed along strike, and regional-scale structures curve to define a recess and salient. In the eastern part of the slate belt, fluid inclusions in syntectonic fibers record fluid temperatures of ~200–260 °C during slaty cleavage formation (Goldstein et al., 2005). As a result, the Taconic slate belt can be used to understand strain variation with depth and within map-view curves in a low-grade metamorphic thrust sheet.

Here we characterize the strain in the Taconic slate belt and interpret it using kinematic models of the internal deformation in thrust sheets. Previous work by Crespi et al. (2010) focused on strain variation in the central and northern parts of the slate belt and concluded that the map-view curvature is a result of the central part having undergone inclined transpression. We build on Crespi et al. (2010) by including strain magnitude data for the entire slate belt and by focusing on strain variation with depth in the thrust sheet. We compare our results to the Taiwan slate belt, where comparable strain data are available, and to observations from thrust sheets metamorphosed at lower and higher temperatures in other orogenic belts.

Geologic Background

The Taconic allochthon is a stack of thrust sheets that lie along the western margin of the Appalachians in westernmost New England and easternmost New York state (Fig. 1). The thrust sheets consist of a Lower Cambrian to Upper Ordovician succession of rift clastics, slope-rise deposits, and synorogenic units (Rowley et al., 1979; Landing, 2012). Transport of the thrust sheets to the west over approximately coeval carbonate platform strata occurred during the final stage of the Early to Late Ordovician Taconic orogeny (Zen, 1961; Rowley and Kidd, 1981; Stanley and Ratcliffe, 1985; Karabinos et al., 1998, 2017; Macdonald et al., 2014, 2017).

The Lower Cambrian to Upper Ordovician succession in the Giddings Brook thrust sheet is dominated by fine-grained siliciclastic rocks. In the western part of the Giddings Brook thrust sheet, the succession consists of eight formations, as described by Rowley et al. (1979) and Landing (2012). Some formations have two names. Although Landing (2012) suggested using the senior synonym, we use both for clarity. The Bomoseen Member of the Nassau Formation, which consists of green wackes with interbedded massive quartzites and green silty slate, was deposited in the Early Cambrian as rift basin fill during breakup of Rodinia. The Truthville Member of the Nassau Formation and the Browns Pond, Mettawee/Middle Granville, Hatch Hill, and Poultney/Deep Kill formations are black, green, purple, or gray slates with variable amounts of interbedded quartz arenites, limestones, and calcareous conglomerates, breccias, and wackes. These Lower Cambrian to Middle Ordovician units were deposited on the slope and rise of the Laurentian passive margin. The rift clastics and passive margin strata are overlain by a sequence of Middle to Upper Ordovician synorogenic deposits consisting of the Indian

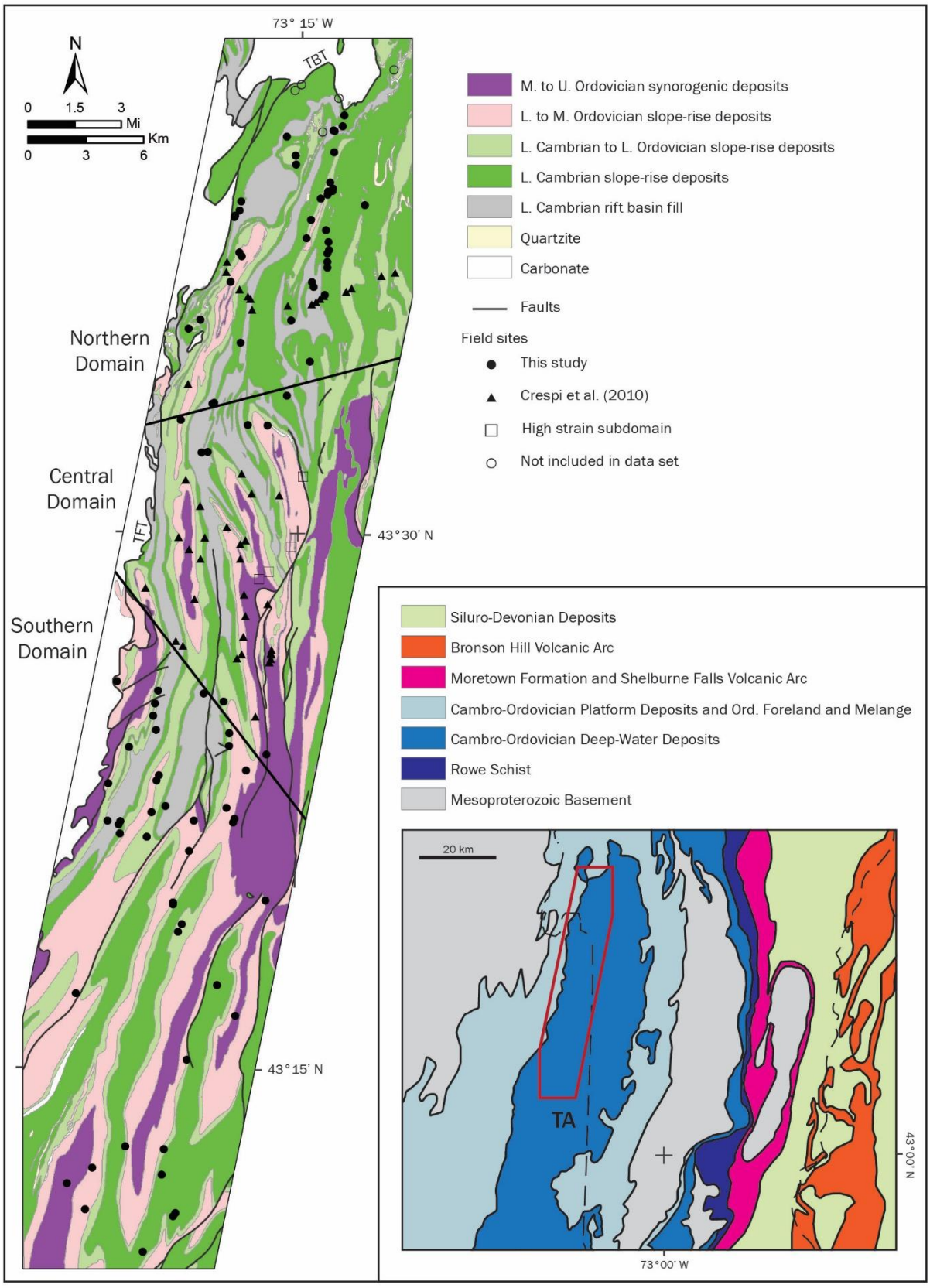
73° 15′ W
N
0 1.5 3
Mi
Km
0 3 6
TBT
Northern Domain
Central Domain
TFT
Southern Domain
43°30′ N
43°15′ N
M. to U. Ordovician synorogenic deposits
L. to M. Ordovician slope-rise deposits
L. Cambrian to L. Ordovician slope-rise deposits
L. Cambrian slope-rise deposits
L. Cambrian rift basin fill
Quartzite
Carbonate
Faults
Field sites
This study
Crespi et al. (2010)
High strain subdomain
Not included in data set
Siluro-Devonian Deposits
Bronson Hill Volcanic Arc
Moretown Formation and Shelburne Falls Volcanic Arc
Cambro-Ordovician Platform Deposits and Ord. Foreland and Melange
Cambro-Ordovician Deep-Water Deposits
Rowe Schist
Mesoproterozoic Basement
20 km
TA
43°00′ N
73°00′ W

Figure 1. Index map of Taconic allochthon in Appalachians (modified from Hibbard et al. (2006)) and generalized geologic map of Taconic slate belt in northern part of Giddings Brook thrust sheet (modified from Ratcliffe et al. (2011)). Lower Cambrian rift basin fill: Bomoseen Member of Nassau Fm. Lower Cambrian slope-rise deposits: Truthville Member of Nassau Fm, Browns Pond Fm, and Mettawee/Middle Granville Fm. Lower Cambrian to Lower Ordovician slope-rise deposits: Hatch Hill Fm. Lower to Middle Ordovician slope-rise deposits: Poultney/Deep Kill Fm. Middle to Upper Ordovician synorogenic deposits: Indian River Fm, Mount Merino Fm, and Pawlet/Austin Glen Fm.

River, Mount Merino, and Pawlet/Austin Glen formations. The Indian River Formation is a red or green-blue slate with minor amounts of interbedded chert and volcanic ash. The Mount Merino Formation consists of chert and black slate. The Pawlet/Austin Glen Formation, which is interpreted as a turbiditic flysch sequence, consists of interbedded greywacke and gray slate.

The Taconic orogeny in the northeastern United States has traditionally been interpreted as resulting from the collision of the eastern margin of the Laurentian continent with a west-facing volcanic arc (Bird and Dewey, 1970; Rowley and Kidd, 1981; Stanley and Ratcliffe, 1985). Karabinos et al. (1998) amended this model to a collision between the Laurentian continent and an older west-facing volcanic arc with a reversal of subduction polarity after the collision and the development of a younger east-facing volcanic arc. This model was further refined using new geochronology data to the current interpretation of a two-stage collision (Macdonald et al., 2014, 2017; Karabinos et al., 2017). During the first stage,

an outboard collision occurred between a fragment of Laurentia and a west-facing volcanic arc built on peri-Gondwanan basement. Continued convergence led to the second stage, during which this composite ribbon terrane collided with the Laurentian continent, accompanied by slab breakoff, a change in subduction polarity, and development of an east-facing volcanic arc. The evolution of this model has also led to the reinterpretation of the Taconic allochthon as a retroarc, rather than a foreland, fold-and-thrust belt emplaced during the end of the second stage.

In the Taconic slate belt, the main phase of deformation is recorded by regional-scale folds, a well-developed slaty cleavage, and a series of out-of-sequence thrust faults (Bosworth and Rowley, 1984; Bosworth et al., 1988). The folds are subhorizontal to gently plunging, tight to isoclinal, and west-vergent. The east-dipping slaty cleavage developed late during folding and is approximately axial planar to the folds. The out-of-sequence thrust faults include the Taconic Frontal thrust, which defines the western edge of the Taconic allochthon, and a series of thrusts generally in the eastern part of the Taconic slate belt. Movement along these faults occurred at the end of the main phase of deformation, after the formation of the folds and slaty cleavage. A later phase of deformation, possibly post-dating Taconic deformation, is recorded by a weak and locally developed crenulation cleavage and associated open to gentle folds (Bosworth and Rowley, 1984; Chan et al., 2000).

Initial displacement of the Taconic allochthon to the west occurred along the Taconic Basal thrust, evidence of which is found in the northernmost part of the Taconic allochthon (Bosworth and Rowley, 1984). The Taconic Basal thrust was folded along with the overlying and underlying rocks during the main phase of deformation. The Taconic Frontal thrust, which

partially follows and cuts through the Taconic Basal thrust, is responsible for the final emplacement of the Taconic allochthon (Bosworth et al., 1988).

Methods

The axial traces of the regional-scale folds in the Taconic slate belt curve, defining a recess in the south and a salient in the north (Fig. 1). We divided the recess and salient into three structural domains: southern, central, and northern. The boundaries between these domains were drawn as straight lines to generally follow the apex of the recess and the apex of the salient. In the southern and northern domains, the fold axial traces trend north-northeast, which is parallel to the overall trend of the Taconic allochthon. In the central domain, the fold axial traces trend north-northwest.

Each domain was characterized by determining the orientation of slaty cleavage, the orientation of the stretching lineation, the sense of shear, and the nature of the strain. Slaty cleavage orientation for each domain was calculated using the mean orientation of slaty cleavage for each field site (Fig. 1). In general, at least five to ten measurements were taken at each field site. Stretching lineation orientation was determined by measuring the preferred orientation of layer silicates on the cleavage surface of hand samples under a binocular microscope. In general, at least five to ten measurements were made at different locations on the cleavage surfaces for each hand sample. In samples where the stretching lineation is poorly expressed or masked by the bedding-cleavage intersection lineation, the long axis of strain fringes in thin section was used to determine the stretching lineation orientation. The sense of shear and nature of the strain were determined from syntectonic fibers composed of layer

silicates and quartz developed on framboids composed of pyrite or iron oxides replacing pyrite or on carbonaceous material with a subspherical shape. Fiber growth was assumed to have been antitaxial because of the compositional difference between the fibers and core objects (Ramsay and Huber, 1983).

To analyze the syntectonic fibers, thin sections were made in two orientations: (1) parallel to slaty cleavage (*XY* plane of strain ellipsoid) and (2) perpendicular to slaty cleavage and parallel to the stretching lineation (*XZ* plane of strain ellipsoid). Both thin section orientations were used to assess the three-dimensional geometry of the fibers. Descriptions for the *XY* plane view down and descriptions for the *XZ* plane view to the north. We used two approaches to measure the stretch ($1 + e = l_f/l_o$ where l_o is the original length and l_f is the final length) along *X* and *Y* depending on the degree of curvature of the fibers. The Durney and Ramsay (1973) technique was used for fibers that are significantly curved. This was the case only for fibers in the *XZ* plane and measurements using the Durney and Ramsay (1973) technique were made in the *XZ* plane to obtain values for $1 + e_1$. For fibers that are straight or only slightly curved, the length of the core object in the *X* or *Y* direction was used as l_o, and the combined length of the core object and fibers in the *X* or *Y* direction was used as l_f. These measurements were primarily made in the *XY* plane to obtain values for both $1 + e_1$ and $1 + e_2$. For some samples, measurements were made in the *XZ* plane to confirm measurements in the *XY* plane are representative.

Results

Southern Domain

The slaty cleavage and stretching lineation orientation data for the southern domain are new to this study (Fig. 1). Measurements of slaty cleavage orientation were obtained from 43 field sites, and measurements of stretching lineation orientation were obtained from 39 of those sites (Table 1).

In the southern domain, slaty cleavage is north-northeast striking and shallowly east dipping, and the stretching lineation is approximately downdip (Figs. 2 and 3). Slaty cleavage has a mean orientation of 013, 32 E, and the stretching lineation has a mean rake of 92 from north and a mean plunge and trend of 35, 105 (Table 2).

Table 1
Site means for slaty cleavage and stretching lineation orientations.

		Cleavage	Stretching Lineation	
Domain	Site	strike, dip	rake	plunge, trend
Southern	HM10	004, 27	81	26, 075
Southern	HM11	002, 37	112	34, 129
Southern	HM12	013, 46	91	45, 103
Southern	HM13	010, 35	125	27, 137
Southern	HM14	004, 45	94	44, 103
Southern	HM15	005, 37	92	35, 099
Southern	HM16	047, 17	–	–
Southern	HM17	026, 16	97	19, 117
Southern	HM18	020, 54	90	55, 104
Southern	HM21	036, 14	–	–
Southern	HM22	350, 14	78	14, 068
Southern	HM23	001, 40	121	35, 130
Southern	HM24	032, 13	88	12, 117
Southern	HM25	021, 32	80	34, 106
Southern	HM26	022, 55	84	60, 092
Southern	HM27	021, 39	80	31, 099
Southern	HM28	002, 40	100	39, 101

Southern	RCC3	021, 14	74	12, 096
Southern	RCC4	005, 17	94	12, 091
Southern	RCC6	017, 33	94	38, 110
Southern	RCC8	037, 40	84	41, 117
Southern	RCC9	023, 29	85	25, 119
Southern	RCC10	013, 39	96	39, 112
Southern	RCC11	357, 39	96	41, 096
Southern	RCC12	343, 25	98	27, 064
Southern	RCC13	016, 32	91	36, 108
Southern	RCC14	017, 45	79	50, 110
Southern	RCC15	009, 32	96	33, 101
Southern	RCC16	017, 30	–	–
Southern	RCC17	016, 42	90	39, 107
Southern	RCC18	353, 29	94	28, 102
Southern	RCC19	027, 26	86	35, 108
Southern	RCC20	026, 46	92	50, 122
Southern	RCC21	013, 29	96	25, 113
Southern	RCC22	347, 32	96	24, 084
Southern	RCC23	007, 25	90	33, 100
Southern	RCC24	029, 26	95	33, 124
Southern	RCC25	018, 32	90	37, 110
Southern	RCC 26	046, 25	71	24, 115
Southern	RCC 27	355, 33	–	–
Southern	RCC 28	013, 41	83	41, 094
Southern	RCC 29	004, 45	100	44, 108
Southern	RCC 30	015, 29	88	29, 103
Central	HRU C	358, 32	113	35, 126
Central	HRU J	010, 36	–	–
Central	HRU B	357, 36	130	20, 132
Central	HRUA	002, 24	–	–
Central	HRUG	005, 27	–	–
Central	HRUH	354, 47	116	41, 122
Central	HRU1	342, 40	–	–
Central	HRU2	010, 42	–	–
Central	HRU4	346, 47	–	–
Central	HRU5	002, 36	139	23, 149
Central	HRU6	352, 32	–	–
Central	HRU7	000, 42	134	28, 148
Central	HRU8	336, 64	120	54, 140
Central	HRU11	340, 49	–	–
Central	HRU14	348, 41	–	–
Central	HRU15	354, 47	–	–
Central	HRU17	339, 51	141	22, 131

Central	HRU19	340, 59	123	39, 110
Central	HRU20	330, 38	–	–
Central	HRU21	003, 59	132	40, 150
Central	HRU22	353, 50	121	32, 129
Central	HRU23	337, 32	143	20, 124
Central	HRU24	329, 58	140	35, 120
Central	HRU26	333, 53	134	40, 121
Central	SR1	009, 46	115	46, 131
Central	SR2	356, 46	–	–
Central	SR3	003, 48	106	49, 130
Central	SR4	358, 46	–	–
Central	SR5	353, 55	140	30, 140
Central	HM1	357, 32	118	27, 122
Central	HM2	001, 13	111	11, 112
Central	HM3	005, 39	97	37, 106
Central	HM4	004, 65	–	–
Central	HM5	345, 53	105	47, 105
Central	HM9	003, 29	108	29, 115
Central	HM19/20	027, 16	115	16, 131
Central	RCC2	007, 53	99	56, 132
High strain	HRUD	017, 44	88	41, 097
High strain	HRU12	011, 29	103	32, 115
High strain	HRU18	005, 47	98	45, 109
High strain	HRU27	358, 38	88	40, 087
Northern	YCC1	350, 31	119	26, 111
Northern	YCC2	025, 36	70	35, 098
Northern	YCC3	001, 30	104	29, 118
Northern	YCC4	355, 22	117	19, 117
Northern	YCC5	019, 29	102	37, 118
Northern	YCC6	010, 29	–	–
Northern	YCC7	018, 34	76	35, 092
Northern	YCC8	022, 34	68	26, 098
Northern	YCC9	025, 30	81	28, 114
Northern	YCC10	001, 21	116	23, 117
Northern	YCC11	012, 27	91	22, 111
Northern	YCC12	009, 18	94	22, 114
Northern	YCC13	008, 28	108	27, 107
Northern	YCC15	357, 25	112	25, 112
Northern	YCC16	011, 27	–	–
Northern	YCC17	355, 23	–	–
Northern	FMT2	015, 33	89	38, 104
Northern	FMT4AB	025, 25	102	28, 120
Northern	FMT4CD	024, 25	93	31, 113

Northern	FMT5	019, 32	–	–
Northern	FMT6	015, 34	93	33, 109
Northern	FMT7	024, 23	95	22, 119
Northern	FMT8	029, 32	93	29, 117
Northern	FMT9	002, 24	93	24, 105
Northern	FMT10	029, 39	121	29, 130
Northern	FMT11	005, 32	–	–
Northern	FMT12ABC	017, 39	–	–
Northern	FMT12DE	019, 42	–	–
Northern	FMT14	034, 23	–	–
Northern	FMT15	358, 36	108	35, 111
Northern	FMT16A	007, 23	93	23, 100
Northern	FMT16B	013, 30	91	31, 103
Northern	FMT17	026, 25	93	27, 121
Northern	FMT18	010, 21	83	20, 093
Northern	FMT19	029, 26	70	21, 108
Northern	FMT20AB	013, 32	102	28, 114
Northern	FMT20CD	008, 27	97	21, 108
Northern	DMT4	034, 33	73	31, 106
Northern	DMT5	005, 24	93	24, 115
Northern	DMT6	009, 13	89	15, 099
Northern	DMT7	008, 35	123	18, 119
Northern	DMT8	014, 33	94	30, 122
Northern	DMT13	014, 19	115	18, 121
Northern	DMT14	016, 46	93	48, 114
Northern	DMT16	019, 40	99	37, 118
Northern	DMT17	019, 19	109	23, 128
Northern	DMT18	009, 16	80	18, 103
Northern	DMT19	028, 37	–	–
Northern	DMT20	013, 15	108	18, 118
Northern	DMT21	340, 30	125	26, 112
Northern	DMT22	352, 29	100	32, 093
Northern	DMT23	009, 21	112	15, 113
Northern	DMT24	010, 20	97	23, 103
Northern	SHS	025, 25	–	–
Northern	HM6/7	024, 38	–	–
Northern	HM8	008, 34	111	34, 133

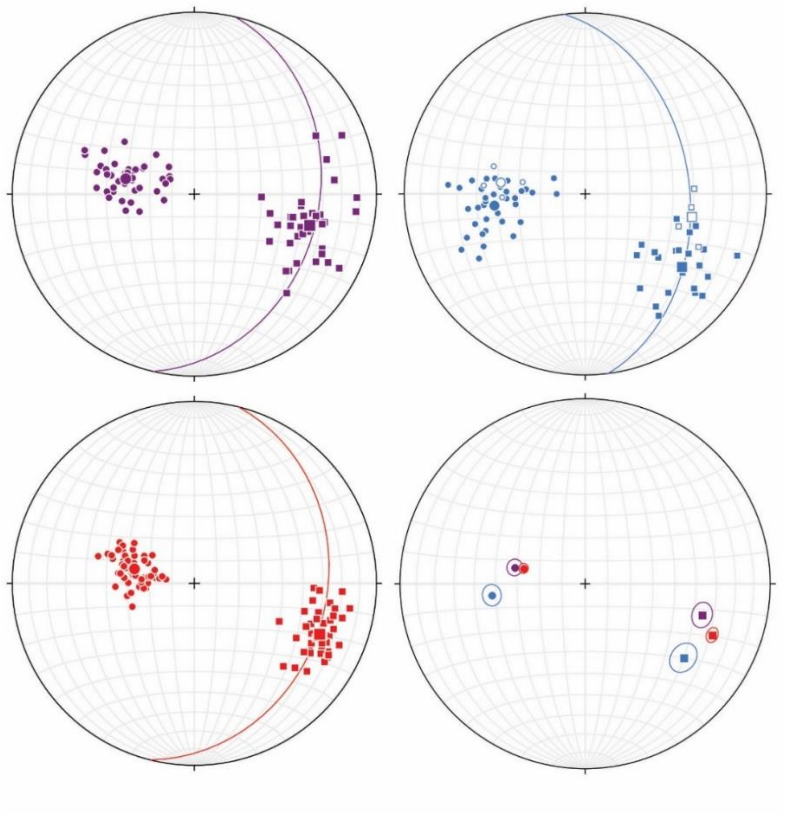

Figure 2. Stereonets of slaty cleavage and stretching lineation for southern (purple), central (blue), and northern (red) domains, and high strain subdomain (hollow blue). Circles: poles to slaty cleavage. Squares: stretching lineation. Larger symbols: means. Great circles: mean slaty cleavage. Small circles: 95% cones of confidence for mean values. Equal-area, lower-hemisphere projections.

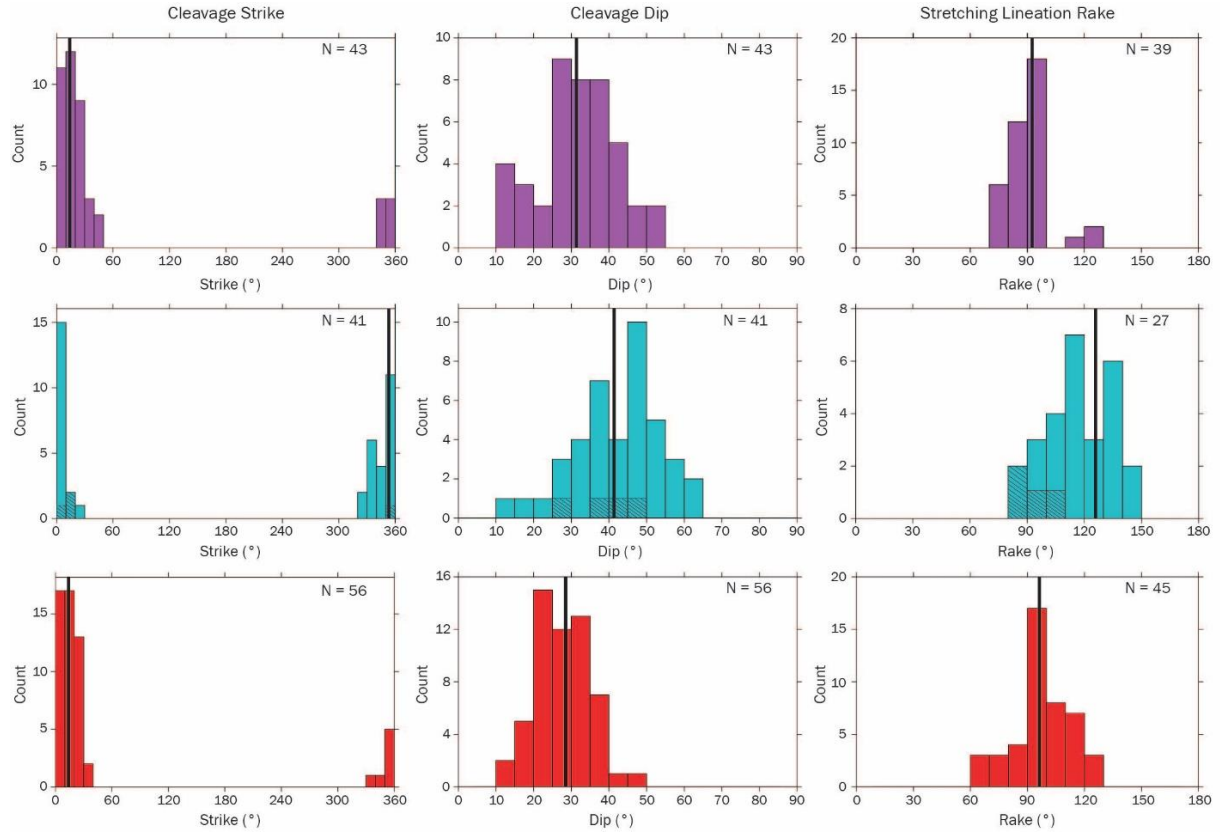

Figure 3. Histograms of slaty cleavage strike, slaty cleavage dip, and stretching lineation rake for southern (purple), central (blue), and northern (red) domains, and high strain subdomain (hatched blue). Black lines: mean values.

Table 2

Domain means for slaty cleavage and stretching lineation orientations and strain values.

	Cleavage	Stretching Lineation				
Domain	strike, dip	rake	plunge, trend	$1 + e_1$	$1 + e_2$	$1 + e_3$*
Southern	013, 32	92	35, 105	1.49	1.10	0.61
Central	353, 42	126	34, 127	1.44	1.06	0.67
Northern	014, 28	97	27, 112	2.28	1.00	0.44

*Calculated assuming constant volume

Strain data were collected from samples from six sites along a generally north-south transect so as to encompass both the along-strike and across-strike extent of the domain (Fig. 4, Table 3). Samples are from both upright and overturned limbs and the hinge zone of regional-scale folds.

In the *XZ* plane, syntectonic fibers are generally straight and either parallel or slightly inclined to slaty cleavage (Fig. 5A). Where inclined, the fibers lie clockwise from the slaty cleavage. Weakly curved fibers are developed on a small proportion of the core objects. With the exception of one site, these fibers curve clockwise when traced from their distal end to the core object. The sense of inclination of the straight fibers and the sense of curvature of the curved fibers are consistent with top-to-west-northwest noncoaxial flow. The site with syntectonic fibers that curve in the opposite sense has a poorly developed crenulation cleavage. This counterclockwise sense of curvature is likely a result of deformation associated with crenulation cleavage development. Some of the core objects at this site also have a short segment of late fiber growth parallel to the incipient crenulation cleavage. In the *XY* plane, the syntectonic fibers are straight (Fig. 5B). Where fiber growth in the *Y* direction is absent, the fibers are parallel to the *X* direction. Where fiber growth in the *Y* direction is present, the fibers are radial in character.

For each site, $1 + e_1$ was determined for both the *XZ* and *XY* sections. The results are essentially the same, giving a mean $1 + e_1$ for the southern domain of 1.49 (Table 2). All the sites exhibit fiber growth in the *Y* direction although the fiber growth is minimal for the northernmost of these sites. The mean $1 + e_2$ for the southern domain is 1.10 (Table 2). All six sites plot relatively close together in the flattening field (Fig. 6).

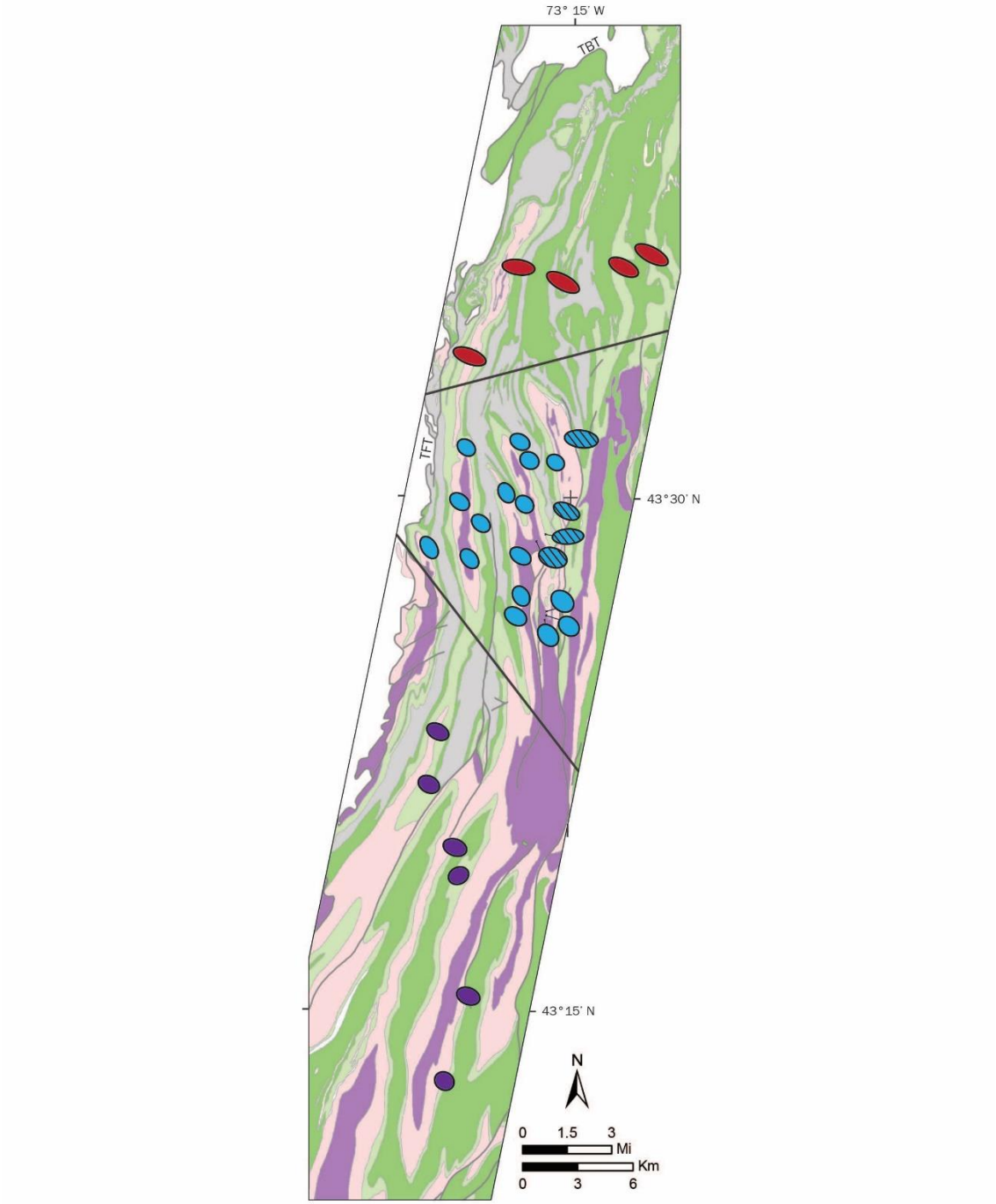

Figure 4. Generalized geologic map of Taconic slate belt in northern part of Giddings Brook thrust sheet (modified from Ratcliffe et al. (2011)) with *XY* planes of strain ellipsoids for southern (purple), central (blue), and northern (red) domains, and high strain subdomain (hatched blue). Ellipses are oriented according to trend of *X*-axis of strain ellipsoid. Legend same as Figure 1.

Table 3

Site means for slaty cleavage dip and strain values.

Domain	Site	Cleavage dip	N*	$1 + e_1$	$1 + e_2$	$1+ e_3$**	*X*/*Y*	*Y*/*Z*	*X*/*Z*
Southern	RCC6	33	35	1.62	1.10	0.56	1.5	2.0	2.9
Southern	RCC10	39	42	1.59	1.10	0.57	1.4	1.9	2.8
Southern	RCC8	40	39	1.47	1.09	0.62	1.3	1.7	2.4
Southern	RCC12	26	48	1.39	1.17	0.61	1.2	1.9	2.3
Southern	RCC24	26	44	1.34	1.17	0.64	1.1	1.8	2.1
Southern	HM17	16	42	1.54	1.02	0.64	1.5	1.6	2.4
Central	HRU B	36	7	1.38	1.00	0.72	1.4	1.4	1.9
Central	HRUC	32	12	1.43	1.00	0.70	1.4	1.4	2.0
Central	HRU H	47	7	1.57	1.10	0.58	1.4	1.9	2.7
Central	HRU 5	36	16	1.41	1.05	0.68	1.3	1.6	2.1
Central	HRU 7	42	7	1.60	1.00	0.63	1.6	1.6	2.6
Central	HRU 8	64	7	1.48	1.00	0.68	1.5	1.5	2.2
Central	HRU 17	51	10	1.30	1.05	0.73	1.2	1.4	1.8
Central	HRU19	59	9	1.47	1.00	0.68	1.5	1.5	2.2
Central	HRU 21	59	5	1.40	1.00	0.71	1.4	1.4	2.0
Central	HRU 22	50	3	1.31	1.00	0.76	1.3	1.3	1.7
Central	HRU 23	32	4	1.25	1.00	0.80	1.3	1.3	1.6
Central	HRU 24	58	11	1.39	1.00	0.72	1.4	1.4	1.9
Central	HRU 26	45	8	1.31	1.09	0.70	1.2	1.6	1.9
Central	SR1	46	10	1.65	1.27	0.48	1.3	2.7	3.5
Central	SR3	48	10	1.49	1.17	0.57	1.3	2.0	2.6
Central	SR5	55	10	1.62	1.20	0.51	1.4	2.3	3.1
High strain	HRU D	44	11	2.24	1.15	0.39	1.9	3.0	5.8
High strain	HRU 12	29	9	1.82	1.00	0.55	1.8	1.8	3.3
High strain	HRU 18	47	25	1.92	1.27	0.41	1.5	3.1	4.7
High strain	HRU 27	42	13	2.07	1.00	0.48	2.1	2.1	4.3
Northern	YCC1	31	32	2.28	1.00	0.44	2.3	2.3	5.2
Northern	YCC2	36	45	2.17	1.00	0.46	2.2	2.2	4.7
Northern	YCC3	30	54	2.38	1.00	0.42	2.4	2.4	5.7
Northern	YCC4	22	10	2.13	1.00	0.47	2.1	2.1	4.5
Northern	YCC5	29	82	2.42	1.00	0.41	2.4	2.4	5.9

*Number of core objects with strain fringes used for strain measurements

**Calculated assuming constant volume

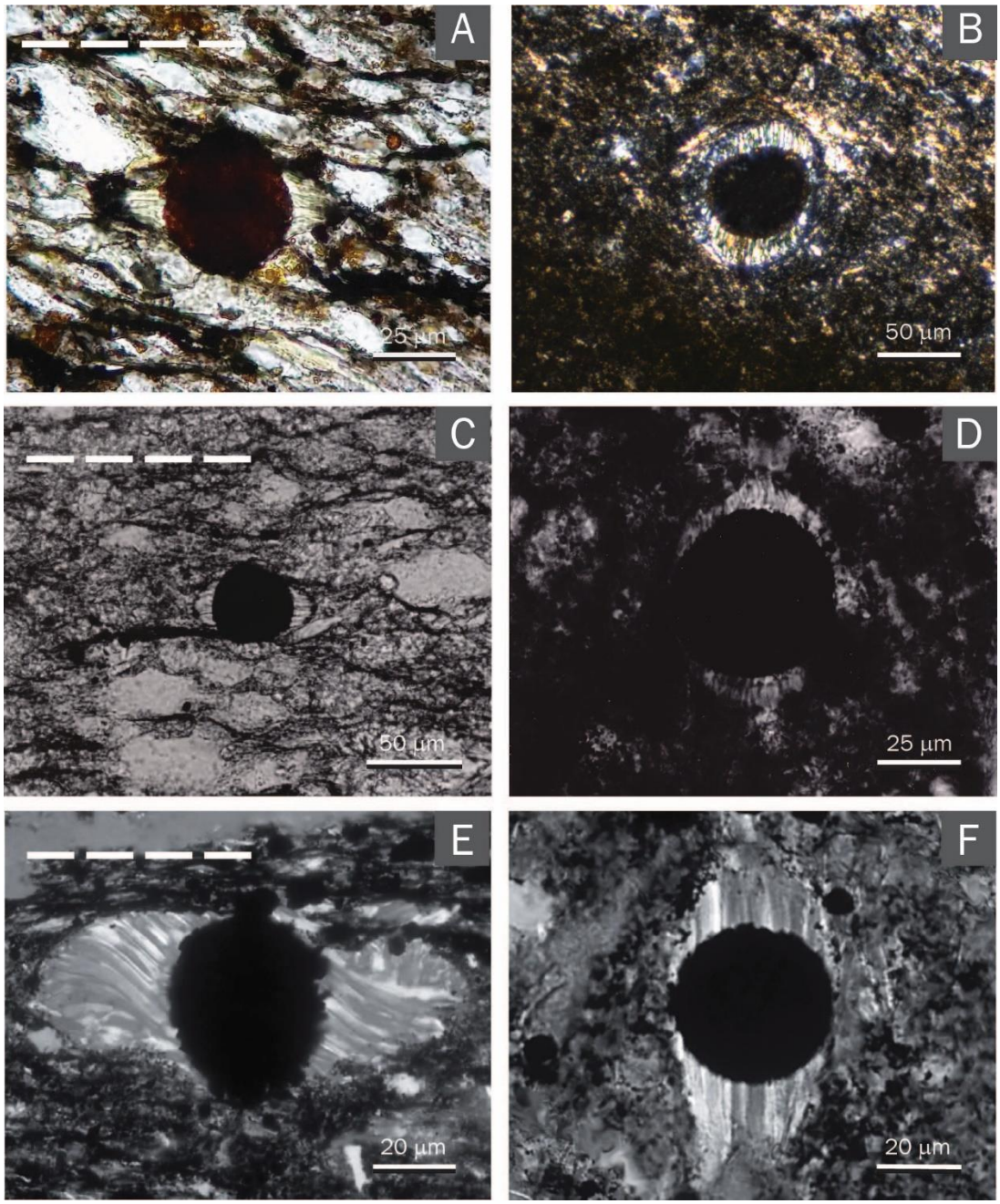

Figure 5. Photomicrographs of syntectonic fibers on subspherical core objects. (A) Southern domain *XZ* section. (B) Southern domain *XY* section. (C) Central domain *XZ* section. (D) Central domain *XY* section. (E) Northern domain *XZ* section. (F) Northern domain *XY* section. A–D: plane-polarized light. E and F: cross-polarized light.

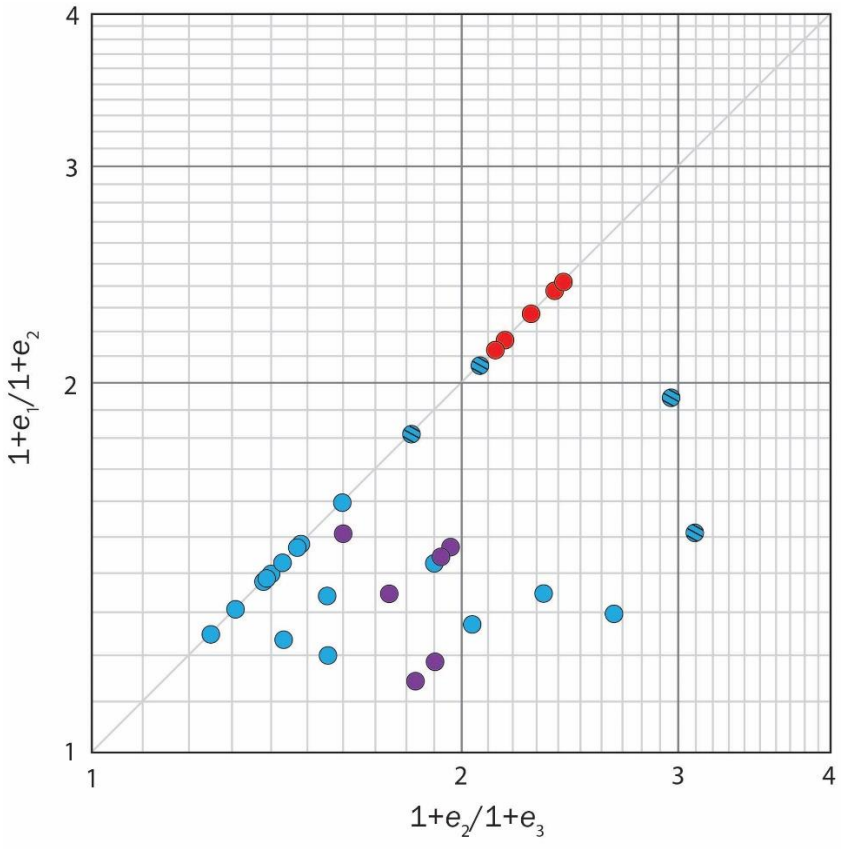

Figure 6. Flinn diagram of strain ellipsoids for southern (purple), central (blue), and northern (red) domains, and high strain subdomain (hatched blue).

Central Domain

We have expanded the dataset for the orientations of slaty cleavage and the stretching lineation in the central domain from that used in Crespi et al. (2010) (Fig. 1). The Crespi et al. (2010) dataset consists of slaty cleavage measurements from 25 sites and stretching lineation measurements from 16 of those sites. The new data are generally from the northern, southern, and eastern edges of the domain. Measurements of the orientation of slaty cleavage from 12 sites and of the stretching lineation from 7 of those sites were added to the Crespi et al. (2010)

dataset (Table 1). Four new sites along the eastern edge of the domain have been separated into a subdomain, the high strain subdomain, of the central domain.

In the central domain, slaty cleavage is north-northwest striking and moderately east dipping, and the stretching lineation rakes moderately from the south (Figs. 2 and 3). Slaty cleavage has a mean orientation of 353, 42 E, and the stretching lineation has a mean rake of 126 from the north and a mean plunge and trend of 34, 127 (Table 2). These results are consistent with those obtained using the Crespi et al. (2010) dataset, supporting the mean orientations being representative of the domain. In the high strain subdomain, the mean orientation of slaty cleavage is 008, 39 E, and the mean orientation of the stretching lineation is 40, 102; the mean rake of the stretching lineation is 94 from the north (Figs. 2 and 3).

Strain data were collected from samples from 16 sites throughout the central domain (Fig. 4, Table 3). This domain was extensively sampled because of the anomalous orientation of the fold axial traces. Samples are from both upright and overturned limbs and the hinge zone of regional-scale folds. In the high strain subdomain, the samples from the four sites are from both upright and overturned limbs of regional-scale folds.

In the *XZ* plane, syntectonic fibers are curved, straight and slightly inclined to slaty cleavage, or straight and parallel to slaty cleavage. Curved fibers curve clockwise when traced from their distal end to the core object, and inclined fibers lie clockwise from the slaty cleavage (Fig. 5C). The sense of curvature of the curved fibers and the sense of inclination of the straight fibers are consistent with top-to-west-northwest noncoaxial flow. In the *XY* plane, the syntectonic fibers are generally straight. Where fiber growth in the *Y* direction is absent, the

fibers are parallel to the *X* direction. Where fiber growth in the *Y* direction is present, the fibers are radial in character. Three sites, however, have fibers that curve in the *XY* plane (Fig. 5D). The sense of curvature is clockwise when traced from the distal end of the fiber to the core object, consistent with a sinistral sense of shear. The main difference between the central domain and the high strain subdomain is that the fiber curvature is greater in the high strain subdomain.

Values for $1 + e_1$ were determined in *XY* sections. The mean $1 + e_1$ for the central domain is 1.44 (Table 2), and the mean $1 + e_1$ for the high strain subdomain is 2.01. The Durney and Ramsay (1973) technique was applied to *XZ* sections from a site in the high strain subdomain with moderately curved fibers. This resulted in a $1 + e_1$ value slightly higher than that obtained from measurements in *XY* sections. Seven of the sites in the central domain and two of the sites in the high strain subdomain have fiber growth in the *Y* direction. The mean $1 + e_2$ for the central domain is 1.06 (Table 2), and the mean $1 + e_2$ for the high strain subdomain is 1.11. Sites in both the central domain and high strain subdomain plot in the flattening field and on the plane strain line (Fig. 6).

Northern Domain

We have also expanded the dataset for the orientations of slaty cleavage and the stretching lineation in the northern domain from that used in Crespi et al. (2010) (Fig. 1). The Crespi et al. (2010) dataset consists of slaty cleavage measurements from 16 sites generally along an east-west transect in the middle of the domain and stretching lineation measurements from 13 of those sites. To improve the distribution of the data in the domain, measurements of

the orientation of slaty cleavage from 40 sites and of the stretching lineation from 32 of those sites were added to the Crespi et al. (2010) dataset. This dataset excludes measurements made at five sites in the very northernmost part of the domain where the dip of cleavage is anomalously steep (Fig. 1).

In the northern domain, slaty cleavage is north-northeast striking and shallowly east dipping, and the stretching lineation is approximately downdip (Figs. 2 and 3). Slaty cleavage has a mean orientation of 014, 28 E, and the stretching lineation has a mean rake of 97 from north and a mean plunge and trend of 27, 112 (Table 2). These results are essentially the same as those obtained using the Crespi et al. (2010) dataset. This consistency supports the mean orientations being representative of the domain.

Strain data were collected from samples from five sites along an east-west transect in the middle of the northern domain (Fig. 4). Samples are from both upright and overturned limbs of regional-scale folds.

In the *XZ* plane, syntectonic fibers are strongly curved (Fig. 5E). When traced from the distal end to the core object, the fibers curve clockwise, which is consistent with top-to-west-northwest noncoaxial flow. Only rarely in this domain are fibers straight and parallel to slaty cleavage. In the *XY* plane, the syntectonic fibers are straight and parallel to the *X* direction (Fig. 5F). No fiber growth was observed in the *Y* direction.

Analysis of syntectonic fibers in *XZ* sections using the Durney and Ramsay (1973) technique yielded a mean $1 + e_1$ for the five samples of 2.28 (Table 2). All five sites plot relatively close together on the plane strain line (Fig. 6).

Synthesis of Results

Interpretation of Structural Domains

The geometry of the syntectonic fibers indicates that the Taconic slate belt is characterized by top-to-west-northwest noncoaxial flow. In each domain, the fibers have the same asymmetry regardless of structural position within a fold. If the fibers were related to folding, they would be expected to be symmetric in fold hinges and to have opposite senses of curvature or inclination to slaty cleavage on upright and overturned limbs. The uniform fiber asymmetry indicates the fibers developed late at the same time as slaty cleavage. The top-to-west-northwest sense of shear indicated by the fibers is consistent with the overall emplacement direction of the Taconic allochthon. This finding suggests that cleavage development was part of a continuum of deformation that began with movement along the Taconic Basal thrust and ended with final emplacement along the Taconic Frontal thrust.

Of the three domains, the southern and northern domains are the most similar. The axial traces of the regional-scale folds are similarly north-northeast trending, and the stretching lineation in both domains plunges down the dip of slaty cleavage. This orthogonal relation can also be seen in the orientation of the long axes of the strain ellipsoids, which lie at high angles to the structural grain (Fig. 4). The main differences between the two domains are the strain magnitude and fiber geometry in the *XZ* plane. Values for $1 + e_1$ are relatively homogeneous within each domain but are significantly higher in the northern domain (Tables 2 and 3). In addition, although fibers are asymmetric in both domains, the degree of asymmetry of the fibers is greater in the northern domain where the fibers are consistently strongly curved.

The central domain differs from the southern and northern domains in several respects. The axial traces of the regional-scale folds trend north-northwest, and the stretching lineation has a moderate rake angle on slaty cleavage. This oblique geometry is also apparent in the orientation of the strain ellipsoids, the long axes of which lie at low to moderate angles to the structural grain (Fig. 4). Strain magnitudes and fiber geometry in the *XZ* plane, however, are similar to that of the southern domain. Like the southern domain, values for $1 + e_1$ in the central domain are relatively homogeneous and significantly lower than those in the northern domain (Tables 2 and 3). In addition, like the southern domain, the degree of fiber asymmetry in the *XZ* plane is less than in the northern domain.

Despite these similarities, the central domain is not a version of the southern domain that has been rotated about a vertical axis. The rotation required to shift slaty cleavage from the southern domain orientation to the central domain orientation results in a downdip, east-northeast plunging *X*-axis, which is contrary to our observations in the central domain. Moreover, evidence for sinistral shear in the *XY* plane is found only in the central domain.

The high strain subdomain does not share the characteristics of the central domain. The stretching lineation is oriented approximately down the dip of the north-northeast-striking slaty cleavage. The $1 + e_1$ values are higher in the high strain subdomain, although generally not as high as the values in the northern domain (Table 3). The high strain subdomain has a greater degree of fiber asymmetry in the *XZ* plane than the central domain, but the fibers are not as consistently strongly curved as they are in the northern domain. All four sites in the high strain subdomain are in close proximity to a zone of out-of-sequence thrust faults, and the subdomain

is interpreted as a localized area of higher strain, separate from the otherwise homogeneous central domain.

The southern and northern domains are described by dip-slip dominated thrusting. This interpretation is supported by the evidence for top-to-west-northwest noncoaxial flow and by the orthogonal relation between the *X* axis and the structural grain. In contrast, the kinematics in the central domain is more complex. Oblique slip is indicated by the evidence for top-to-west-northwest noncoaxial flow in the *XZ* plane and sinistral shear in the *XY* plane and by the moderate rake of the *X* axis on slaty cleavage. Based on these characteristics, the central domain has been interpreted as a region of inclined transpression (Crespi et al., 2010).

Structural Levels in Giddings Brook Thrust Sheet

The northern part of the Giddings Brook thrust sheet plunges gently to the south. As a result, the southern domain is at a higher structural level than the northern domain (Fig. 7). This geometry is evidenced by the along-strike changes in stratigraphic units exposed at the surface and by the mapped location of the Taconic Basal thrust (Fig. 1). The age of exposed stratigraphic units generally decreases from north to south. For example, the Lower Cambrian rift basin fill is significantly more exposed in the northern domain compared to the southern domain. In addition, the Middle to Upper Ordovician synorogenic deposits are extensively exposed in the southern domain but are not present in the northern domain. The Taconic Basal thrust is mapped only in the northernmost part of the Giddings Brook thrust sheet where it marks the contact between allochthonous and parautochthonous rocks and around the William Miller Chapel window in the northern domain (Rowley, 1983; Bosworth and Rowley, 1984).

Based on the approximate thickness of the stratigraphic succession and the along-strike length of the Taconic slate belt, the northern part of the Giddings Brook thrust sheet plunges south about 1–2°.

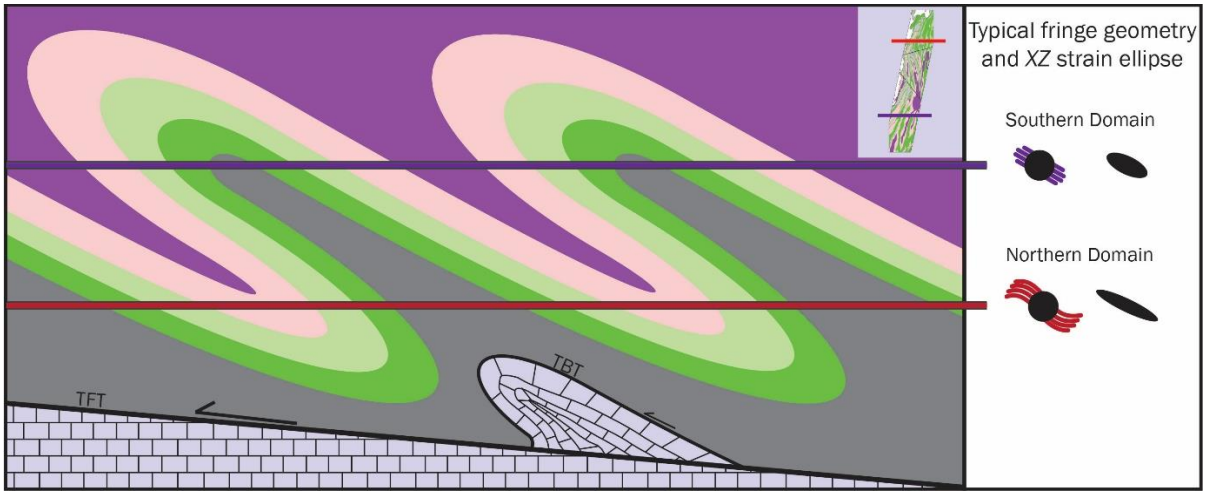

Figure 7. Schematic diagram illustrating structural levels of southern and northern domains of northern part of Giddings Brook thrust sheet. Inset: strain ellipse and generalized syntectonic fiber geometry in *XZ* plane for southern (purple) and northern (red) domains.

The higher structural level southern domain is characterized by low magnitude strain and a low degree of fiber asymmetry, and the lower structural level northern domain is characterized by high magnitude strain and a high degree of fiber asymmetry. These characteristics indicate a decreasing strain gradient normal to the base of the Giddings Brook thrust sheet. The central domain does not conform to this strain gradient, further supporting its interpretation as an anomalous region of inclined transpression.

Kinematic Model for Southern and Northern Domains

Because the southern and northern domains are dominated by dip-slip thrusting, the strain distribution can be analyzed using two-dimensional kinematic models of thrust sheet deformation. These models use concepts developed for shear zones while allowing a discontinuity between the deforming material in the thrust sheet and the footwall. Deformation in the thrust sheet is described by simple shear, combined simple shear and volume change, or combined simple shear and pure shear (Ramsay, 1980; Coward and Kim, 1981; Kligfield et al., 1981; Sanderson, 1982; Fossen and Tikoff, 1993; Tikoff and Fossen, 1993). The simple shear component increases toward the base of the thrust sheet, as illustrated by Sanderson (1982). The volume change component is oriented normal to the base of the thrust sheet, volume loss resulting in thinning of the thrust sheet and volume gain resulting in thickening of the thrust sheet. The pure shear component consists of extension or shortening parallel to the thrust in the transport direction. The former results in thinning of the thrust sheet, and the latter results in thickening of the thrust sheet. These models are typically represented in an R_{XZ} versus θ' graph.

Values for $1 + e_3$ are needed to determine R_{XZ}, and the dip of the thrust sheet is needed to determine θ'. Volume change must be considered when calculating $1 + e_3$. Goldstein et al. (1995) used reduction spots in the Taconic slate belt to estimate volume change during slaty cleavage development. They concluded that the rocks underwent heterogeneous volume loss, with the most highly strained sites recording at least 55% volume loss. Goldstein et al. (1998) obtained similar results using the thecal spacing of graptolites. Our strain data from syntectonic fibers, however, are not entirely consistent with Goldstein et al.'s (1995, 1998) results. For

example, reduction spots indicate heterogeneous strain within hand samples, within sites, and between sites while the strain obtained from syntectonic fibers is homogeneous at these scales. In addition, the graptolite thecal spacing yields constrictional strain in three of the five sites, which lie in an area where the syntectonic fibers record flattening and plane strain. Therefore, when determining $1 + e_3$, we consider the argument for large volume loss and constant volume and compare both results to our observations. We use a value of 5° ± 5° east for the dip of the thrust sheet. This value is consistent with the map expression of the trace of the Taconic Frontal thrust and numerous cross sections of the northern Taconic allochthon (Rowley et al., 1979; Bosworth and Rowley, 1984; Bosworth et al., 1988; Hayman and Kidd, 2002).

A significant amount of volume loss, such as the minimum 55% estimated by Goldstein et al. (1995), results in a value of 19.7 for R_{XZ} in the northern domain, which places the domain in the volume gain field of an R_{XZ} versus θ' graph. A lower cleavage dip than observed is needed for the mean values to plot on the appropriate volume loss curve. This discrepancy argues against large volume loss in the Taconic slate belt.

On an R_{XZ} versus θ' graph for combined simple shear and volume change, when assuming constant volume, the mean values for the northern domain plot essentially on the simple shear curve, and the mean values for the southern domain plot between the 10% and 20% volume loss curves (Fig. 8). Consistent with the higher degree of fiber asymmetry, the northern domain is characterized by higher shear strain than the southern domain. The position of the northern domain on the simple shear curve agrees with evidence from syntectonic fibers for plane strain and our assumption of constant volume. The southern domain plots in the volume loss field but close to the simple shear curve. The small amount of volume loss

indicated may be compensated by the observed extension in the *Y* direction, which is not accounted for in this two-dimensional kinematic model.

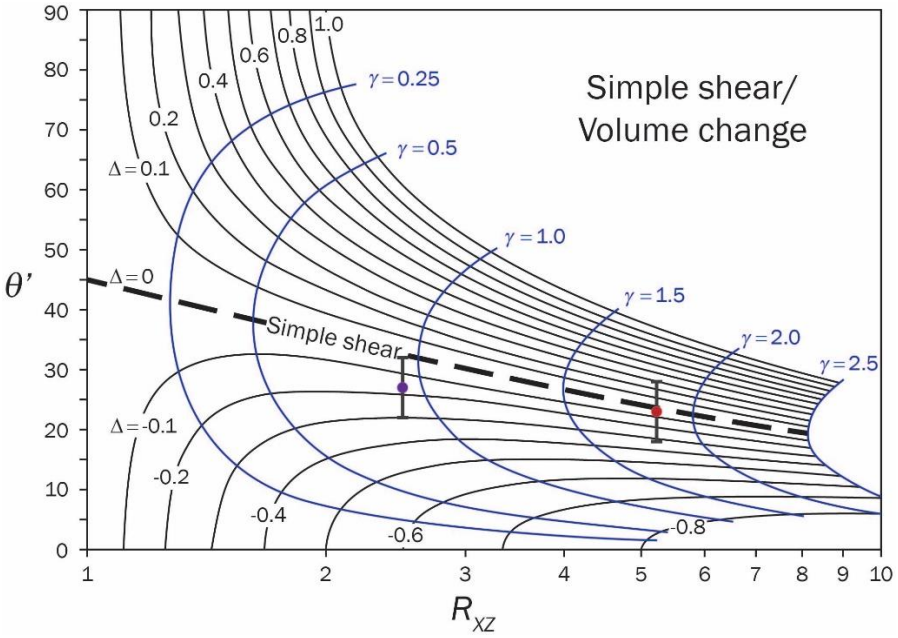

Figure 8. R_{XZ} versus θ' graph for simultaneous simple shear and volume change (after Fossen and Tikoff (1993)). R_{XZ}: strain ratio in *XZ* plane. θ': angle between long axis of strain ellipsoid and base of thrust sheet. γ: shear strain. Δ: volume change. Purple dot: southern domain with 5° dip of base of thrust sheet. Red dot: northern domain with 5° dip of base of thrust sheet. Vertical bars: ± 5° for dip of base of thrust sheet.

Discussion

Tectonic Significance for Taconic Orogeny

The transport direction of the Taconic allochthon has long been assumed to be orthogonal to the overall north-northeast trend of the allochthon. For example, Bradley (1989)

palinspastically restored the Taconic allochthon using an azimuth of 105°. The evidence for this transport direction consists of the overall nature of the thrust belt geometry (Bosworth and Rowley, 1984; Bosworth et al., 1988) and the east-southeast trend of rotated fold hinge lines in mélange in the footwall of the Taconic Frontal thrust (Bosworth and Vollmer, 1981).

Our stretching lineation data provide an additional approach for estimating the transport direction of the Taconic allochthon. The geometry of the syntectonic fibers suggests slaty cleavage and the stretching lineation formed during noncoaxial flow as the Taconic allochthon was being emplaced. The trend of the *X*-axis, i.e., stretching lineation, can be used as a proxy for the trend of the shear direction if there is no kinematic partitioning of strain within a domain and if the deformation is two-dimensional, i.e., the vorticity vector does not rotate. A lack of kinematic partitioning in the domains of the Taconic slate belt is supported by the homogeneity of the strain within each domain. The 127° trend of the stretching lineation in the central domain cannot be used to determine the transport direction because this domain is an area of inclined transpression. However, the 105° and 112° trends of the stretching lineation in the dip-slip dominated southern and northern domains provide a good estimate for the transport direction. This east-southeast transport direction is consistent with the inference of previous workers (Bosworth and Vollmer, 1981; Bradley, 1989).

The dip-slip character of the southern and northern domains is unlikely to be a result of kinematic partitioning at the orogen-scale into orogen-perpendicular and orogen-parallel components. Major strike-slip faults have not been mapped between the Taconic allochthon and Bronson Hill volcanic arc, the east-facing arc formed after the second stage collision (Fig. 1)

(Ratcliffe et al., 2011). Thus, the Taconic orogeny, or at least the latter part when the Taconic allochthon was emplaced, is likely a consequence of nearly orthogonal plate convergence.

Comparison to External and Internal Thrust Sheets

Previous studies that have applied kinematic models to the internal deformation of thrust sheets have found evidence for thrust sheet thickening in relatively competent and/or unmetamorphosed to weakly metamorphosed strata and evidence for thrust sheet thinning in weak lithologies and/or highly metamorphosed strata. Thrust sheet thickening has been inferred, for example, for quartzites in the Moine thrust zone in Scotland (Coward and Kim, 1981), quartzites in the upper part of the Willard thrust sheet in the Idaho–Utah–Wyoming thrust belt (Yonkee, 2005), and the unmetamorphosed Neka Valley nappe complex in Iran (Nabavi et al., 2017). In addition, thrust-parallel shortening has been inferred for many external thrust sheets (Mitra, 1994; Long et al., 2011; Weil and Yonkee, 2012). Thrust sheet thinning has been inferred, for example, for greywackes in the lower and basal levels of the Willard thrust sheet (Yonkee, 2005), the Himalayan thrust sheets of Bhutan (Long et al., 2011), marble breccias in a shear zone in the Northern Apennines, Italy (Kligfield et al., 1981), and mylonites in the Moine thrust zone (Sanderson, 1982). After documenting both modes of internal deformation in the Himalayan thrust sheets of Bhutan, Long et al. (2011) proposed that the minimum temperature for quartz plasticity (~250-300 °C) controls the transition from thrust sheet thickening in external thrust sheets to thrust sheet thinning in internal thrust sheets.

Our work in the Taconic slate belt adds to the study of the internal deformation of thrust sheets by documenting the variation in strain in a low-grade metamorphic thrust sheet

that lies in the transition between external and internal thrust sheets. Pressure solution is the dominant deformation mechanism in the slates, with fluid temperatures during slaty cleavage formation of ~200-260 °C (Goldstein et al., 2005). The lack of evidence for significant thrust sheet thinning in the Taconic slate belt is consistent with Long et al.'s (2011) proposal that thrust sheet thinning is characteristic of thrust sheets metamorphosed above the minimum temperature for quartz plasticity. Moreover, our results from the Taconic slate belt suggest that simple shear characterizes the transition between external and internal thrust sheets, at least in thrust sheets dominated by relatively incompetent strata (Fig. 9).

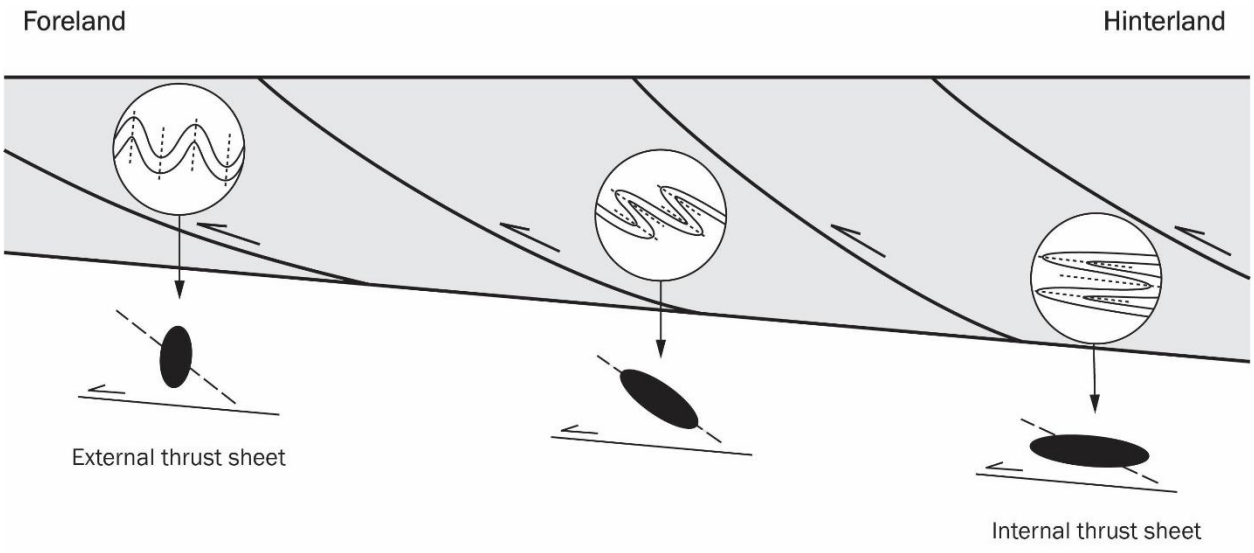

Figure 9: Schematic diagram of orogenic wedge showing strain variation from external to internal thrust sheets. Black ellipses and dashed lines: *XZ* planes of strain ellipsoid and orientations of *X*-axis for simple shear alone.

Comparison to Taiwan Slate Belt

Strain data from the Taiwan slate belt further supports simple shear characterizing the transition between external and internal thrust sheets. The Taiwan slate belt lies in the west-vergent prowedge of the active Taiwan orogenic belt, which is a result of the collision between the Luzon volcanic arc and the Chinese continental margin (Byrne et al., 2011). Structural and strain data have been obtained from different structural levels in this slate belt along the Southern Cross Island Highway (Tillman and Byrne, 1995). Here a west-vergent, out-of-sequence thrust fault has placed strata deformed at a lower structural level above strata deformed at a higher structural level. These areas are referred to as the western domain (higher structural level) and eastern domain (lower structural level). Tillman and Byrne (1995) presented slaty cleavage and stretching lineation orientation data together with strain data obtained from syntectonic fibers formed around pyrite framboids for both domains.

The western and eastern domains of the Taiwan slate belt share characteristics with the southern and northern domains of the Taconic slate belt. In Taiwan, slaty cleavage strikes north-northeast, parallel to the overall structural grain of the orogen, and the stretching lineation plunges downdip. In *XY* sections, syntectonic fibers indicate plane strain. In *XZ* sections, syntectonic fibers are curved and have the same sense of curvature regardless of structural position within a fold. The curvature is consistent with top-to-west-northwest noncoaxial flow. Moreover, like the Taconic slate belt, the strain magnitude is greater and the slaty cleavage dip is lower in the domain at a lower structural level compared to the domain at a higher structural level.

For the western domain, the mean $1 + e_1$ value is 1.64 and the mean cleavage dip is 65° E. For the eastern domain, the mean $1 + e_1$ value is 3.70 and the mean cleavage dip is 45° E. We assume constant volume to calculate $1 + e_3$ and R_{XZ}, which yields 0.61 and 2.69, respectively, for the western domain and 0.27 and 13.69, respectively, for the eastern domain. To determine θ', we assume the base of the thrust sheet is horizontal, which yields 65° for the western domain and 45° for the eastern domain.

These two pairs of values for R_{XZ} and θ' plot significantly above the simple shear curve, implying the strata within the thrust sheet underwent volume gain or thrust-parallel shortening. Volume gain in slates, however, is highly unlikely, and other workers who have documented thrust-parallel shortening in thrust sheets report low R_{XZ} values of about 1.5 to 2 (Coward and Kim, 1981; Yonkee, 2005). One possibility is that the western and eastern domains have been rotated clockwise (north viewing) which would steepen slaty cleavage. For the R_{XZ} values to lie on the simple shear curve, the mean slaty cleavage dip would need to be 35° shallower in the western domain and 30° shallower in the eastern domain. This difference in slaty cleavage dip can be explained by rotation related to displacement along an out-of-sequence thrust fault. The Tulungwan fault, which forms the western boundary of the Taiwan slate belt along the Southern Cross Island Highway, is the northern part of the active Tulungwan-Chaochou fault system. In the hanging wall of the southern Tulungwan fault, Huang and Byrne (2014) documented a post-cleavage, regional-scale antiform plunging approximately 30° to the south-southwest with a steep to overturned northwest limb, evidenced by folded cleavage. In their model for the formation of the antiform, initial fault-bend folding is followed by trishear folding, with slaty cleavage rotating clockwise to steeper dips during movement

over the ramp. Thus, a steepening of slaty cleavage along the Southern Cross Island Highway from rotation related to fault motion is plausible.

The possibility of post-cleavage deformation in the Taiwan slate belt along the Southern Cross Island Highway complicates interpretation of the strain data. Thrust sheet thinning is unlikely because it would require rotations larger than expected from movement over a ramp. Thrust sheet thickening may also be absent, depending on the amount of post-cleavage deformation. The lack of evidence for thrust sheet thinning and the likelihood of clockwise rotation of cleavage suggest that the Taiwan slate belt along the Southern Cross Island Highway may be dominated by simple shear, like the southern and northern domains of the Taconic slate belt. Furthermore, given that the Taiwan slate belt is a low-grade metamorphic thrust sheet, this interpretation is additional support for simple shear as characteristic of the transition from external to internal thrust sheets.

Conclusions

The Taconic slate belt in the northern part of the Giddings Brook thrust sheet is described by three structural domains. All three domains are characterized by top-to-west-northwest noncoaxial flow. In the southern and northern domains, the structural grain trends parallel to the overall north-northeast trend of the Taconic allochthon. Our analyses indicate that these domains are dominated by dip-slip thrusting with the strain increasing toward the base of the thrust sheet. In contrast, the central domain has an anomalous north-northwest-trending structural grain. Our results agree with the interpretation of Crespi et al. (2010) that this domain is a region of inclined transpression. The stretching lineation plunges approximately

down the dip of slaty cleavage in the southern and northern domains but is moderately raking on slaty cleavage in the central domain. Moreover, the stretching lineation in the central domain is obliquely oriented with respect to the overall structural grain of the domain. The higher structural level southern domain has lower strain magnitude than the lower structural level northern domain, while the strain magnitude in the central domain is not as predicted for this region based on the strain gradient given by the southern and northern domains. Finally, the degree of fiber asymmetry is less in the higher structural level southern domain than in the lower structural level northern domain.

The along-strike and with-depth variations of strain between the three structural domains in the Taconic slate belt reflect the structural evolution of a low-grade metamorphic thrust sheet. The strain magnitude and slaty cleavage dip in the northern domain are consistent with simple shear if the thrust sheet dips about 5° east. The strain magnitude and slaty cleavage dip in the southern domain imply simple shear combined with small amounts of volume loss, which was likely accommodated by the observed along-strike extension in this domain. Similar work on internal deformation in unmetamorphosed to weakly metamorphosed external thrust sheets has generally shown thrust sheet thickening accommodated by thrust-parallel shortening (Coward and Kim, 1981; Yonkee, 2005; Nabavi et al., 2017). Moreover, work in higher-grade metamorphic internal thrust sheets has generally shown that the internal deformation is described by large amounts of thrust sheet thinning accommodated by thrust-parallel extension and/or volume loss (Kligfield et al., 1981; Sanderson, 1982; Yonkee, 2005; Long et al., 2011). The results of this study show the transition between external and internal

thrust sheets may be characterized by simple shear with no significant thrust sheet thickening or thinning.

References

Bird, J.M., Dewey, J.F., 1970. Lithosphere plate–continental margin tectonics and the evolution of the Appalachian orogen. Geol. Soc. Am. Bull. 81, 1031–1060. https://doi.org/10.1130/0016-7606(1970)81[1031:LPMTAT]2.0.CO;2

Bosworth, W., Vollmer, F.W., 1981. Structures of the medial Ordovician flysch of eastern New York: deformation of synorogenic deposits in an overthrust environment. J. Geol. 89, 551–568. https://doi.org/10.1086/628622

Bosworth, W., Rowley, D.B., 1984. Early obduction-related deformation features of the Taconic Allochthon: analogy with structures observed in modern trench environments. Geol. Soc. Am. Bull. 95, 559–567. https://doi.org/10.1130/0016-7606(1984)95<559:EODFOT>2.0.CO;2

Bosworth, W., Rowley, D.B., Kidd, W.S.F., Steinhardt, C., 1988. Geometry and style of post-obduction thrusting in a Paleozoic orogen: the Taconic Frontal Thrust System. J. Geol. 96, 163–180. https://doi.org/10.1086/629207

Bradley, D.C., 1989, Taconic plate kinematics as revealed by foredeep stratigraphy, Appalachian orogen: Tectonics 8, 1037–1049. https://doi.org /10.1029/TC008i005p01037.

Byrne, T., Chan, Y.-C., Rau, R.-J., Lu, C.-Y., Lee, Y.-H., Wang, Y.-J., 2011. The arc–continent collision in Taiwan. In: Brown, D., Ryan, P.D. (Eds.), Arc–Continent Collision. Springer, Berlin, Heidelberg, 213–245. https://doi.org/10.1007/978-3-540-88558-0_8

Chan, Y.C., Crespi, J.M., and Hodges, K.V., 2000. Dating cleavage formation in slates and phyllites with the 40Ar/39Ar laser microprobe: An example from the western New England Appalachians, U.S.A.: Terra Nova 12, 264–271, https://doi.org/10.1046/j.1365-3121.2000.00308.x

Coward, M.P., Kim, J.H., 1981. Strain within thrust sheets. In: McClay, K.R., Price, N.J. (Eds.), Thrust and Nappe Tectonics 9, Geological Society, London, Special Publications, 275–292. https://doi.org/10.1144/GSL.SP.1981.009.01.25

Coward, M.P., Potts, G.J., 1983. Complex strain patterns developed at the frontal and lateral tips to shear zones and thrust zones. J. Geol. 5, 383–399, https://doi.org/10.1016/0191-8141(83)90025-1

Crespi, J.M., Underwood, H.R., Chan, Y.-C., 2010. Orogenic curvature in the northern Taconic allochthon and its relation to footwall geometry. In: Tollo, R.P., Bartholomew, M.J., Hibbard, J.P., Karabinos, P.M. (Eds.), From Rodinia to Pangea: the Lithotectonic Record of

the Appalachian Region, vol. 206. Geological Society of America Memoirs, pp. 111–122. https://doi.org/10.1130/2010.1206(06).

Durney, D.W., Ramsay, J.G., 1973. Incremental strains measured by syntectonic crystal growths. In: De Jong, K.A., Scholten, R., (Eds.), Gravity and Tectonics. John Wiley and Sons, New York, pp. 67–96.

Fossen, H., Tikoff, B., 1993. The deformation matrix for simultaneous simple shearing, pure shearing and volume change, and its application to transpression-transtension tectonics. J. Struct. Geol. 15, 413–422. https://doi.org/10.1016/0191-8141(93)90137-Y

Goldstein, A., Knight, J., Kimball, K., 1998. Deformed graptolites, finite strain and volume loss during cleavage formation in rocks of the Taconic slate belt, New York and Vermont, U.S.A. J. Struct. Geol. 20, 1769–1782. https://doi.org/10.1016/S0191-8141(98)00083-2

Goldstein, A., Pickens, J., Klepeis, K., Linn, F., 1995. Finite strain heterogeneity and volume loss in slates of the Taconic Allochthon, Vermont, U.S.A. J. Struct. Geol. 17, 1207–1216. https://doi.org/10.1016/0191-8141(95)00022-6

Goldstein, A., Selleck, B., Valley, J.W., 2005. Pressure, temperature, and composition history of syntectonic fluids in a low-grade metamorphic terrane. Geology 33, 421–424. https://doi.org/10.1130/G21143.1

Hayman, N.W., Kidd, W.S.F., 2002. Reactivation of prethrusting, synconvergence normal faults as ramps within the Ordovician Champlain-Taconic thrust system. Geol. Soc. Am. Bull. 114, 476–489. https://doi.org/10.1130/0016-7606(2002)114<0476:ROPSNF>2.0.CO;2

Hibbard, J.P., van Staal, C.R., Rankin, D.W., Williams, H., 2006. Lithotectonic map of the Appalachian Orogen, Canada–United States of America. "A" Series Map 2096A. Geological Survey of Canada. https://doi.org/10.4095/221932

Huang, C., Byrne, T.B., 2014. Tectonic evolution of an active tectonostratigraphic boundary in accretionary wedge: An example from the Tulungwan-Chaochou Fault system, southern Taiwan. J. Struct. Geol. 69, 320–333. https://doi.org/10.1016/j.jsg.2014.06.007

Karabinos, P., Samson, S.D., Hepburn, J.C., Stoll, H.M., 1998. The Taconian orogeny in the New England Appalachians: collision between Laurentia and the Shelburne Falls arc. Geology 26, 215–218. https://doi.org/10.1130/0091-7613(1998)026<0215:TOITNE>2.3.CO;2

Karabinos, P., MacDonald, F.A., Crowley, J.L., 2017. Bridging the gap between the foreland and hinterland I: geochronology and plate tectonic geometry of Ordovician magmatism and terrane accretion on the Laurentian margin of New England. Am. J. Sci. 317, 515–554. https://doi.org/10.2475/05.2017.01

Kligfield, R., Carmignani, L., Owens, W.H., 1981. Strain analysis of a Northern Apennine shear zone using deformed marble breccias. J. Struct. Geol. 3, 421–436. https://doi.org/10.1016/0191-8141(81)90042-0

Landing, E., 2012. The great American carbonate bank in eastern Laurentia: its births, deaths, and linkage to paleooceanic oxygenation (Early Cambrian–Late Ordovician). In: Derby, J.R., Fritz, R.D., Longacre, S.A., Morgan, W.A., Sternbach, C.A. (Eds.), The Great American Carbonate Bank: the Geology and Economic Resources of the Cambrian–Ordovician Sauk Megasequence of Laurentia, vol. 98. American Association of Petroleum Geologists Memoirs, pp. 451–492. https://doi.org/10.1306/13331502M983502

Long, S., McQuarrie, N., Tobgay, T., Hawthorne, J., 2011. Quantifying internal strain and deformation temperature in the eastern Himalaya, Bhutan: implications for the evolution of strain in thrust sheets. J. Struct. Geol. 33, 579–608. https://doi.org/10.1016/j.jsg.2010.12.011

Macdonald, F.A., Ryan-Davis, J., Coish, R.A., Crowley, J.L., Karabinos, P., 2014. A newly identified Gondwanan terrane in the northern Appalachian Mountains: implications for the Taconic orogeny and closure of the Iapetus Ocean. Geology 42, 539–542. https://doi.org/10.1130/G35659.1

Macdonald, F.A., Karabinos, P.M., Crowley, J.L., Hodgin, E.B., Crockford, P.W., Delano, J.W., 2017. Bridging the gap between the foreland and hinterland II: geochronology and tectonic setting of Ordovician magmatism and basin formation on the Laurentian margin of New England and Newfoundland. Am. J. Sci. 317, 555–596. https://doi.org/10.2475/05.2017.02

Mitra, G., 1994. Strain variation in thrust sheets across the Sevier fold-and-thrust belt (Idaho-Utah-Wyoming): implications for section restoration and wedge taper evolution. J. Struct. Geol. 16, 585–602. https://doi.org/10.1016/0191-8141(94)90099-X

Nabavi, S.T., Rahimi-Chakdel, A., Khademi, M., 2017. Structural pattern and emplacement mechanism of the Neka Valley nappe complex , eastern Alborz , Iran. Int. J. Earth Sci. 106, 2387–2405. https://doi.org/10.1007/s00531-016-1433-x

Ramsay, J.G., 1980. Shear zone geometry: a review. J. Struct. Geol. 2, 83–99. https://doi.org/10.1016/0191-8141(80)90038-3

Ramsay, J.G., Huber, M.I., 1983. The Techniques of Modern Structural Geology: Volume 1. Strain Analysis. Academic Press, London, United Kingdom.

Ratcliffe, N.M., Stanley, R.S., Gale, M.H., Thompson, P.J., and Walsh, G.J., 2011. Bedrock geologic map of Vermont: U.S. Geological Survey Scientific Investigations Map 3184, 3 sheets, scale 1:100,000

Rowley, D.B., Kidd, W.S.F., Delano, L.L., 1979. Detailed stratigraphic and structural features of the Giddings Brook slice of the Taconic allochthon in the Granville area. In: Friedman, G. (Ed.), Field Trip Guidebook for the 51st Annual Meeting of the New York State Geological Association and 71st New England Intercollegiate Geological Conference. Rensselaer Polytechnic Institute, Troy, New York, pp. 186–242.

Rowley, D.B., Kidd, W.S.F., 1981. Stratigraphic relationships and detrital composition of the medial Ordovician flysch of western New England: implications for the tectonic evolution of the Taconic orogeny. J. Geol. 89, 199–218. https://doi.org/10.1086/628580

Rowley, D.B., 1983. Operation of the Wilson Cycle during the Early Paleozoic Evolution of the Northern Appalachians: with Emphasis on the Stratigraphy, Structure, and Emplacement History of the Taconic Allochthon. Unpublished PhD thesis, State University of New York at Albany.

Sanderson, D.J., 1982. Models of strain variation in nappes and thrust sheets: a review. Tectonophysics 88, 201–233. https://doi.org/10.1016/0040-1951(82)90237-2

Stanley, R.S., Ratcliffe, N.M., 1985. Tectonic synthesis of the Taconian orogeny in western New England. Geol. Soc. Am. Bull. 96, 1227–1250. https://doi.org/10.1130/0016-7606(1985)96<1227

Tikoff, B., Fossen, H., 1993. Simultaneous pure and simple shear: the unifying deformation matrix. Tectonophysics 217, 267–283. https://doi.org/10.1016/0040-1951(93)90010-H

Tillman, K.S., Byrne, T.B., 1995. Kinematic analysis of the Taiwan Slate Belt. Tectonics 14, 322–341. https://doi.org/10.1029/94TC02451

Weil, A.B., Yonkee, W.A., 2012. Layer-parallel shortening across the Sevier fold-thrust belt and Laramide foreland of Wyoming: spatial and temporal evolution of a complex geodynamic system. Earth Planet. Sci. Lett. 357–358, 405–420. https://doi.org/10.1016/j.epsl.2012.09.021

Yonkee, A., 2005. Strain patterns within part of the Willard thrust sheet, Idaho–Utah–Wyoming thrust belt. J. Struct. Geol. 27, 1315–1343. https://doi.org/10.1016/j.jsg.2004.06.014

Zen, E-an, 1961. Stratigraphy and structure at the north end of the Taconic Range in west-central Vermont. Geol. Soc. Am. Bull. 72, 293–338. https://doi.org/10.1130/0016-7606(1961)72[293:SASATN]2.0.CO;2

Zen, E-an, 1967. Time and space relationships of the Taconic allochthon and autochthon. Geological Society of America Special Paper 97, 107 p. https://doi.org/10.1130/SPE97-p1

Appendix I: Field site Locations and slaty cleavage measurements

	Coordinates		Cleavage		
Site	Lat	Long	Strike	Dip	Mean
RCC2	43.397100°	-73.269120°			007/53
			026	57	
			012	56	
			008	54	
			011	54	
			005	57	
			351	50	
			356	49	
RCC3	43.365307°	-73.290145°			021/14
			022	12	
			015	09	
			016	10	
			021	15	
			022	17	
			025	12	
			014	15	
			029	17	
			016	15	
			025	15	
			022	16	
RCC4	43.366976°	-73.289234°			005/17
			357	12	
			004	18	
			005	16	
			007	18	
			004	17	
			009	14	
			358	22	
			016	17	
RCC6	43.327570°	-73.327950°			017/33
			021	33	
			026	23	
			011	40	
			015	42	
			011	23	
			015	39	
			024	33	
RCC8	43.358010°	-73.345230°			037/40
			035	41	
			037	43	
			038	42	
			037	39	
			038	40	
			040	41	
			043	35	
			036	44	

			040	39	
			035	44	
			043	37	
			031	42	
			032	39	
			036	41	
			036	37	
			035	40	
RCC9	43.326732°	-73.327984°			023/29
			034	25	
			032	27	
			023	31	
			019	28	
			011	35	
RCC10	43.254196°	-73.318211°			013/39
			014	39	
			011	42	
			016	43	
			015	37	
			009	41	
			010	36	
			012	38	
			018	40	
			007	38	
			013	39	
RCC11	43.18119°	-73.32604°			358/39
			005	39	
			350	42	
			355	38	
			011	39	
			009	32	
			006	36	
			359	33	
			010	30	
			355	46	
			354	51	
			347	50	
			346	43	
			354	31	
			355	40	
			358	41	
			335	38	
			018	37	
RCC12	43.31368°	-73.32491°			343/26
			325	27	
			346	30	
			343	31	
			355	30	
			353	23	
			001	25	

			341	21	
			336	26	
			345	23	
			324	24	
RCC13	43.200556°	-73.333383°			016/32
			017	36	
			019	35	
			015	30	
			013	30	
RCC14	43.182763°	-73.324501°			017/45
			013	44	
			028	50	
			012	43	
			015	44	
RCC15	43.365253°	-73.362198°			009/32
			006	30	
			010	32	
			010	27	
			001	27	
			004	33	
			010	39	
			008	45	
			012	24	
			009	34	
			007	32	
			010	37	
			006	31	
			015	29	
			020	26	
			020	30	
			002	36	
RCC16	43.363757°	-73.363141°			017/30
			025	25	
			032	31	
			022	18	
			003	30	
			007	31	
			022	39	
			013	33	
			011	37	
RCC17	43.359452°	-73.362356°			016/42
			017	39	
			027	40	
			013	42	
			021	44	
			012	44	
			010	46	
			008	41	
			015	46	
			017	39	

RCC18	43.35168°	-73.317986°			353/29
			346	27	
			347	24	
			358	25	
			350	30	
			354	30	
			351	37	
			007	28	
RCC19	43.36579°	-73.31516°			027/26
			018	24	
			039	26	
			020	24	
			031	22	
			024	27	
			030	31	
			026	24	
			029	25	
			023	35	
RCC20	43.274851°	-73.287466°			026/46
			036	50	
			029	50	
			012	54	
			027	38	
			027	40	
			023	36	
			016	47	
			021	43	
			027	46	
			029	53	
			033	47	
RCC21	43.289127°	-73.299396°			013/29
			005	30	
			016	26	
			010	36	
			008	37	
			018	31	
			017	33	
			017	25	
			024	28	
			004	24	
			017	25	
RCC22	43.317635°	-73.322176°			347/32
			357	25	
			354	32	
			348	26	
			348	26	
			352	22	
			003	32	
			354	39	
			354	35	

			353	38	
			330	40	
			331	36	
			330	37	
			343	43	
			353	30	
			345	26	
			349	21	
			353	35	
			346	32	
RCC23	43.284703°	-73.389295°			007/25
			342	15	
			339	12	
			354	19	
			340	22	
			355	22	
			351	21	
			011	30	
			017	27	
			011	39	
			030	26	
			027	28	
			019	37	
			007	32	
			011	34	
RCC24	43.21254°	-73.33223°			029/26
			027	21	
			029	25	
			030	25	
			033	26	
			028	33	
RCC25	43.328822°	-73.268785°			018/32
			022	35	
			021	31	
			016	23	
			021	31	
			016	33	
			020	32	
			016	34	
			019	34	
			012	29	
			020	37	
RCC 26	43.164674°	-73.344534°			046/25
			039	26	
			046	25	
			053	24	
			044	29	
			056	20	
			042	26	
			041	30	

			043	27	
			043	23	
RCC 27	43.184016°	-73.381770°			355/33
			354	36	
			357	31	
RCC 28	43.196235°	-73.393803°			013/41
			027	23	
			011	42	
			033	38	
			000	40	
			011	42	
			359	36	
			014	51	
			022	41	
			009	53	
			025	35	
			008	46	
			022	42	
			359	39	
RCC 29	43.203694°	-73.378331°			004/45
			003	45	
			005	45	
			004	45	
			007	45	
			008	49	
			358	42	
			001	44	
RCC 30	43.213575°	-73.357305°			015/29
			022	29	
			007	27	
			016	29	
			022	32	
			023	27	
			013	31	
			019	31	
			005	30	

Appendix II: Site locations and stretching lineation measurements

Site	Coordinates Lat	Long	Sample: Name Cleavage: strike, dip	Rake	Mean rake	plunge, trend
RCC2	43.397100°	-73.269120°	JR180517_TA1		99	56, 132
			026, 57	109		
				108		
				123		
				96		
				92		
				83		
				107		
				80		
				78		
				104		
				107		
RCC3	43.365307°	-73.290145°	JR180517_TA2		74	12, 096
			022, 12	74		
				73		
				55		
				83		
				63		
				72		
				104		
				68		
				72		
				74		
RCC4	43.366976°	-73.289234°	JR180517_TA3		94	12, 091
			357, 12	111		
				92		
				109		
				94		
				99		
				90		
				78		
				86		
				90		
				88		
RCC6	43.327570°	-73.327950°	JR250617_TA4		94	38, 110
			015, 38	99		
				96		
				93		
				90		
				88		
				99		
				94		
				101		
				84		
				97		
RCC8	43.358010°	-73.345230°	JR250617_TA6		84	41, 117

			035, 41	84 87 85 86 91 82 82 77 85 78		
RCC9	43.326732°	-73.327984°	JR260617_TA7 034, 25	88 95 95 89 87 73 75 90 76 83	85	25, 119
RCC10	43.254196°	-73.318211°	JR260617_TA8 014, 39	95 83 110 90 107 104 100 90 108 77	96	36, 112
RCC11	43.18119°	-73.32604°	JR260617_TA9 005, 39	96 102 102 101 101 104 104 103 107 109	103	38, 112
			JR260617_TA1 0 350, 42	70 92 88 92 95 92 94	89	42, 079

				93 87 82 77 92 98		
RCC12	43.31368°	-73.32491°	JR260617_TA11 325, 27	75 77 90 125 88 118 110 110 85 106	98	27, 064
RCC13	43.200556°	-73.333383°	JR140817_TA12 017, 36	102 85 90 100 90 95 78 78 88 99 95	91	36,108
RCC14	43.182763°	-73.324501°	JR140817_TA13 037, 51	79 81 79 74 78 74 81 85 81 80	79	50, 110
RCC15	43.365253°	-73.362198°	JR150817_TA14 006, 30	108 97 98 102 101 87 96 97	99	30,106

				100 102		
			JR150817_TA15 002, 36		93	36,096
				77 82 88 109 97 97 103 91 93 97		
RCC17	43.359452°	-73.362356°	JR150817_TA16 017, 39		90	39,107
				92 96 93 83 86 90 92 91 83		
RCC18	43.35168°	-73.317986°	JR150817_TA17 007, 28		94	28, 102
				106 94 88 100 83 87 91 107 97 85		
RCC19	43.36579°	-73.31516°	JR150817_TA18 023, 35		86	35,108
				78 94 75 85 99 82 74 89 97 86		
RCC20	43.274851°	-73.287466°	JR150817_TA19 029, 50		92	50, 122
				90 91 90 90		

				93 90 108 104 85 79		
RCC21	43.289127°	-73.299396°	JR150817_TA20 017, 25	98 97 84 93 93 97 104 99 90 106	96	25, 113
RCC22	43.317635°	-73.322176°	JR160817_TA22 345, 26	88 87 95 106 102 101 93 112 87 113 79 100	97	26, 083
			JR160817_TA23 349, 21	84 88 86 95 106 100 99 102 88 101	95	21, 084
RCC23	43.284703°	-73.389295°	JR160817_TA2 5 007, 32	69 101 84 94 109 99 80 77	89	32, 096

				90 85		
			JR160817_TA26 011, 34		92	34, 103
				90 101 95 87 93 90 90 91 91 94 93		
RCC24	43.21254°	-73.33223°	JR160817_TA28 033, 26		95	33, 124
				91 109 95 96 89 89 89 92 97 93 109		
RCC25	43.328822°	-73.268785°	JR160817_TA29 028, 33		90	37,110
				110 86 89 75 86 116 79 93 90 89 83 84		
RCC 26	43.164674°	-73.344534°	JR160817_TA30 039, 26		71	24, 115
				72 64 75 58 66 69 69 70 92		

RCC 28	43.196235°	-73.393803°	JR160817_TA31027, 23	77 73 77 91 86 88 68 83 79 90 96	83	41, 094
RCC 29	43.203694°	-73.378331°	JR160817_TA35003, 45	92 104 96 109 88 96 91 109 108 106	100	44, 108
RCC 30	43.213575°	-73.357305°	JR160817_TA36022, 29	85 87 77 90 93 77 79 101 96 91	88	29, 103

Appendix III: Syntectonic fiber measurements for southern domain

Site-Sample	T.S. Coordinates									
Thin section	X	Y	Size (μm)	X l_o	X l_f	X stretch	Rake X	Y l_o	Y l_f	Y stretch
RCC6-TA4	58.4	13.0	32.5	11.5	18.5	1.61	90	11.50	12.50	1.09
TA4-z-2	48.5	18.8	47.0	11	16.5	1.50	81	11.00	12.00	1.09
	51.4	21.6	54.0	15	25	1.67	110	17.00	19.00	1.12
	51.4	21.5	53.8	14	19	1.36	107	15.00	17.00	1.13
	49.4	22.0	55.0	24	38	1.58	108	25.00	29.00	1.16
	49.0	22.2	55.5	17	28	1.65	105	18.00	20.00	1.11
	49.0	22.5	56.3	16	24	1.50	89	17.50	19.00	1.09
	48.9	22.4	56.0	12.5	21	1.68	83	12.00	14.00	1.17
	48.7	22.4	56.0	15.5	22.5	1.45	102	14.00	15.00	1.07
	48.7	22.5	56.3	16	24	1.50	109	14.50	18.00	1.24
	48.5	22.7	56.8	19	32	1.68	109	21.50	22.00	1.02
	48.3	22.7	56.8	16	24	1.50	113	16.50	16.50	1.00
	48.3	22.8	57.0	13	23.5	1.81	108	15.50	16.00	1.03
	48.2	22.7	56.8	23	34	1.48	107	23.50	24.00	1.02
	48.2	22.8	57.0	13	23	1.77	112	15.00	15.00	1.00
	48.0	22.8	57.0	17.5	30.5	1.74	106	17.50	20.00	1.14
	47.9	23.8	59.5	17	27	1.59	91	19.00	21.00	1.11
	44.7	23.0	57.5	15	22.5	1.50	71	14.00	17.00	1.21
	39.4	22.4	56.0	9.5	15	1.58	81	10.00	10.50	1.05
	42.9	22.3	55.8	9	14	1.56	70	10.00	12.00	1.20
Means			39.8			1.58	98			1.10
	X	Y	size (μm)	X l_o	X l_f	X stretch				
TA4-y-1	65.3	20.3	38.8	15.50	28.00	1.81				
	63.9	20.0	16.3	6.50	11.50	1.77				
	63.8	19.9	18.8	7.50	11.00	1.47				
	64.3	20.3	12.5	5.00	8.50	1.70				
	65.0	21.0	15.0	6.00	10.00	1.67				
	67.8	21.1	40.0	16.00	23.50	1.47				
	70.0	19.5	17.5	7.00	8.50	1.21				
	70.3	19.2	17.5	7.00	12.50	1.79				
	70.2	17.1	27.5	11.00	19.00	1.73				
	65.9	11.9	18.8	7.50	13.00	1.73				
	63.4	15.8	40.0	16.00	31.00	1.94				
	40.7	15.0	12.5	5.00	9.00	1.80				
	40.9	15.0	12.5	5.00	7.00	1.40				
	64.5	20.8	12.5	5.00	9.00	1.80				
	64.9	20.8	12.5	5.00	9.00	1.80				
Means			20.8			1.67				
RCC8-TA6	X	Y	size (μm)	X l_o	X l_f	X stretch	Rake X	Y l_o	Y l_f	Y stretch
TA6-z-1	70.0	7.0	15.0	6.00	9.00	1.50	80	6.00	7.00	1.17
	66.9	17.0	32.5	13.00	20.00	1.54	85	13.00	14.00	1.08
	40.0	24.1	10.0	4.00	6.00	1.50	79	4.00	4.50	1.13
	40.3	19.0	10.0	4.00	6.00	1.50	88	4.00	4.50	1.13
	41.4	8.0	10.0	5.00	7.50	1.50	83	5.00	5.00	1.00
	41.6	12.8	12.5	5.00	7.00	1.40	86	6.00	6.50	1.08

	43.3	23.0	15.0	6.00	8.00	1.33	99	6.00	6.50	1.08
	47.0	24.2	12.5	5.00	7.00	1.40	82	5.00	6.00	1.20
	43.5	8.7	10.0	4.00	6.00	1.50	98	4.00	4.50	1.13
	44.5	21.1	11.3	4.50	6.00	1.33	81	5.00	5.00	1.00
	48.4	20.0	12.5	5.00	7.00	1.40	82	5.00	5.50	1.10
	49.4	21.0	10.0	4.00	6.00	1.50	100	4.00	4.00	1.00
	50.4	23.7	11.3	4.50	7.00	1.56	98	4.50	4.50	1.00
	51.4	21.4	11.3	4.50	7.00	1.56	80	5.00	5.50	1.10
	53.0	22.1	12.5	5.00	7.50	1.50	100	5.00	6.00	1.20
	52.5	22.4	12.5	5.00	8.00	1.60	90	5.00	5.50	1.10
	55.2	22.8	12.5	5.00	7.00	1.40	78	5.00	5.00	1.00
	55.0	22.7	10.0	4.00	6.00	1.50	87	4.00	5.00	1.25
	54.9	16.0	17.5	7.00	9.50	1.36	94	6.00	6.00	1.00
Means			13.1			1.47	88			1.09
	X	Y	size (μm)	X l_o	X l_f	X stretch	Rake X	Y l_o	Y l_f	Y stretch
TA6-z-2	47.0	8.4	17.5	7.00	11.00	1.57	101	7.00	7.50	1.07
	50.0	10.0	21.3	8.50	11.50	1.35	84	9.00	10.00	1.11
	64.4	12.7	17.5	7.00	10.00	1.43	97	7.00	7.50	1.07
	53.8	13.2	15.0	4.00	6.00	1.50	95	4.00	4.75	1.19
Means			17.8			1.46	94			1.11
	X	Y	size (μm)	X l_o	X l_f	X stretch				
TA6-y-1	40.3	23.1	16.3	6.50	9.00	1.38				
	40.4	19.0	11.3	4.50	6.50	1.44				
	40.5	16.0	10.0	4.00	6.00	1.50				
	42.3	12.2	10.0	4.00	6.00	1.50				
	41.9	12.0	10.0	4.00	6.00	1.50				
Means			11.5			1.47				
	X	Y	size (μm)	X l_o	X l_f	X stretch				
TA6-y-2	39.8	15.5	10.0	4.00	6.00	1.50				
	41.4	19.4	10.0	4.00	6.00	1.50				
	41.5	5.7	15.0	6.00	9.00	1.50				
	42.0	6.4	22.5	9.00	13.00	1.44				
	42.0	15.8	10.0	4.00	6.00	1.50				
	42.0	22.2	10.0	4.00	5.50	1.38				
	44.6	12.3	11.3	4.50	6.50	1.44				
	44.7	18.5	15.0	6.00	9.00	1.50				
	45.0	18.5	12.5	5.00	7.00	1.40				
	44.8	18.4	12.5	5.00	7.50	1.50				
	44.8	18.7	13.8	4.75	7.00	1.47				
Means			13.0			1.47				
RCC10-TA8	X	Y	size (μm)	X l_o	X l_f	X stretch	Rake X	Y l_o	Y l_f	Y stretch
TA8-z-3	40.5	2.9	27.5	11.00	17.00	1.55	92	11.00	13.00	1.18
	69.6	19.2	52.5	23.00	38.00	1.65	93	21.00	23.00	1.10
	68.7	19.9	87.5	34.00	48.00	1.41	94	35.00	35.00	1.00
	68.8	16.2	71.3	27.50	46.50	1.69	85	28.50	31.00	1.09
	68.8	16.1	42.5	18.00	25.50	1.42	95	17.00	19.50	1.15
	68.9	16.2	77.5	29.00	45.00	1.55	87	31.00	31.50	1.02
	69.3	15.9	66.3	22.00	36.00	1.64	89	26.50	27.50	1.04
	70.0	15.0	77.5	26.50	43.00	1.62	90	31.00	31.00	1.00
	70.2	15.3	86.3	32.00	49.50	1.55	91	34.50	38.00	1.10

	66.4	9.9	37.5	15.00	22.00	1.47	98	15.00	17.00	1.13
	65.6	12.8	37.5	16.00	25.50	1.59	105	15.00	16.50	1.10
	66.9	15.9	60.0	25.00	40.00	1.60	90	24.00	24.50	1.02
	67.0	17.8	57.5	25.50	42.00	1.65	84	23.00	25.00	1.09
	65.9	21.8	50.0	17.50	29.00	1.66	88	20.00	21.50	1.08
	65.2	16.5	75.0	29.00	42.00	1.45	92	30.00	30.00	1.00
	64.6	8.7	52.5	22.00	32.00	1.45	96	21.00	22.00	1.05
	64.0	24.8	50.0	19.00	32.00	1.68	92	20.00	21.00	1.05
	62.5	14.7	60.0	24.00	35.00	1.46	107	24.00	25.00	1.04
	61.3	19.5	30.0	12.50	20.00	1.60	95	12.00	15.00	1.25
	61.9	23.4	56.3	24.50	37.00	1.51	88	22.50	23.00	1.02
Means			57.8			1.56	93			1.07
	X	Y	size (μm)	X l_o	X l_f	X stretch				
TA8-y-6	41.5	14.6	22.5	9.00	15.00	1.67				
	43.8	14.7	22.5	9.00	14.00	1.56				
	44.1	14.9	20.0	8.00	12.50	1.56				
	44.0	14.6	20.0	8.00	11.00	1.38				
	54.7	15.5	27.5	11.00	18.00	1.64				
	15.1	15.6	15.0	6.00	10.50	1.75				
	55.0	15.2	18.8	7.50	11.50	1.53				
	59.6	15.7	16.3	6.50	11.00	1.69				
	60.1	15.0	35.0	14.00	24.00	1.71				
	59.3	14.8	65.0	26.00	47.00	1.81				
	66.8	15.0	22.5	9.00	13.00	1.44				
	64.2	14.6	16.3	6.50	11.50	1.77				
	60.8	14.6	15.0	6.00	10.00	1.67				
	49.9	14.7	13.8	5.50	8.50	1.55				
	41.5	14.1	17.5	7.00	11.50	1.64				
	44.5	14.4	40.0	16.00	27.00	1.69				
	49.0	14.2	10.0	4.00	6.00	1.50				
	50.0	14.0	13.8	5.50	9.00	1.64				
	51.3	14.2	17.5	7.00	10.50	1.50				
	54.0	14.0	25.0	10.00	16.50	1.65				
	56.4	14.0	22.5	9.00	16.00	1.78				
	65.5	11.1	57.5	23.00	38.00	1.65				
Means			24.3			1.63				
RCC12-TA11	X	Y	size (μm)	X l_o	X l_f	X stretch	Rake X	Y l_o	Y l_f	Y stretch
TA11-z-2	39.7	7.1	15.0	6.50	9.50	1.46	43	6.00	8.00	1.33
	X	Y	size (μm)	X l_o	X l_f	X stretch	Rake X	Y l_o	Y l_f	Y stretch
TA11-z-4	44.7	14.1	7.5	3.00	4.00	1.33	55	3.00	3.50	1.17
	40.4	20.0	7.5	3.00	4.50	1.50	85	3.00	4.00	1.33
	40.0	20.5	7.5	3.00	4.00	1.33	78	3.00	3.50	1.17
	39.7	20.6	8.8	3.00	5.00	1.67	54	3.50	4.00	1.14
	40.0	24.0	8.8	4.00	5.00	1.25	102	3.50	3.50	1.00
	42.1	18.6	16.3	6.50	9.00	1.38	N/A	6.50	9.00	1.38
	42.0	18.7	7.5	3.00	4.00	1.33	84	3.00	3.25	1.08
	42.6	22.5	7.5	3.00	4.00	1.33	N/A	3.00	4.00	1.33
	42.8	18.1	12.5	5.00	6.50	1.30	80	5.00	6.00	1.20
	43.0	19.3	7.5	3.00	4.50	1.50	71	3.00	3.25	1.08
	43.1	20.6	25.0	10.00	15.00	1.50	78	16.50	18.00	1.09

	45.0	15.0	17.5	7.00	10.00	1.43	80	7.00	8.00	1.14
	47.4	17.0	15.0	6.00	7.50	1.25	61	6.00	6.50	1.08
	49.5	17.2	12.5	5.50	8.00	1.45	60	5.00	5.50	1.10
	50.6	15.3	13.8	5.00	6.50	1.30	62	5.50	6.00	1.09
	51.4	20.0	25.0	11.00	14.50	1.32	60	10.00	11.00	1.10
	57.3	10.1	13.8	6.00	8.00	1.33	52	5.50	6.50	1.18
	60.9	14.8	13.8	5.00	6.50	1.30	N/A	5.00	6.50	1.30
	61.5	16.3	15.0	6.00	8.00	1.33	71	6.00	7.50	1.25
	65.8	8.0	17.5	7.00	9.50	1.36	81	7.00	8.00	1.14
Means			13.0			1.38	71			1.17
	X	Y	size (μm)	X l_o	X l_f	X stretch				
TA11-y-2	47.6	14.2	32.5	13.00	16.50	1.27				
	69.9	5.3	13.8	5.50	8.00	1.45				
	60.5	7.1	16.3	6.50	8.00	1.23				
	57.2	7.7	27.5	11.00	14.00	1.27				
	88.2	7.1	15.0	6.00	8.00	1.33				
	41.5	15.5	12.5	5.00	7.50	1.50				
Means			19.6			1.34				
	X	Y	size (μm)	X l_o	X l_f	X stretch				
TA11-y-3	41.9	11.2	8.1	3.25	4.50	1.38				
	42.1	11.2	7.5	3.00	4.00	1.33				
	41.8	11.6	10.0	4.00	5.00	1.25				
	42.4	13.1	8.8	3.50	5.50	1.57				
	41.9	14.0	13.8	5.50	7.50	1.36				
	39.5	16.7	7.5	3.00	5.00	1.67				
	45.3	17.0	7.5	3.00	5.00	1.67				
	46.1	15.7	12.5	5.00	7.00	1.40				
	46.2	11.4	20.0	8.00	11.00	1.38				
	47.0	12.6	7.5	3.00	4.00	1.33				
	47.0	15.0	22.5	9.00	11.50	1.28				
	47.4	14.7	10.0	4.00	6.00	1.50				
	49.3	17.0	15.0	6.00	8.00	1.33				
	49.5	17.2	10.0	4.00	5.00	1.25				
	49.8	12.8	10.0	4.00	6.00	1.50				
	50.6	15.0	8.8	4.00	6.00	1.50				
	51.4	13.3	20.0	8.00	11.00	1.38				
	52.4	14.7	22.5	9.00	12.00	1.33				
	53.1	15.7	10.0	4.00	6.00	1.50				
	54.6	15.1	20.0	8.00	12.50	1.56				
	55.4	16.7	13.8	5.50	7.00	1.27				
	55.4	15.4	15.0	6.00	8.00	1.33				
	55.7	14.7	25.0	10.00	13.00	1.30				
	58.0	17.0	12.5	5.00	7.00	1.40				
	62.0	14.6	17.5	7.00	10.00	1.43				
Means			13.4			1.41				
RCC24-TA28	X	Y	size (μm)	X l_o	X l_f	X stretch	Rake X	Y l_o	Y l_f	Y stretch
TA28-z-1	49.5	3.0	10.0	4.00	6.00	1.50	150	4.00	5.00	1.25
	51.6	17.3	16.3	7.00	8.00	1.14	84	6.50	7.00	1.08
	51.6	17.2	13.8	5.50	6.50	1.18	N/A	5.50	6.50	1.18
	52.0	17.6	20.0	8.00	9.50	1.19	95	6.00	7.00	1.17

	54.6	3.0	20.0	8.00	10.00	1.25	97	8.00	8.50	1.06
	55.5	4.3	13.8	5.50	7.00	1.27	N/A	5.50	7.00	1.27
	55.5	7.3	18.8	6.00	8.00	1.33	96	7.70	9.00	1.17
	58.2	2.9	13.8	5.50	6.00	1.09	N/A	5.50	6.00	1.09
	58.9	5.1	15.0	6.00	7.00	1.17	N/A	6.00	7.00	1.17
	62.8	6.6	30.0	12.00	14.00	1.17	N/A	12.00	14.00	1.17
	63.0	10.7	22.5	9.00	12.00	1.33	65	9.00	11.00	1.22
	63.1	10.7	17.5	7.00	9.50	1.36	60	7.00	8.00	1.14
	62.8	12.8	16.3	6.50	8.50	1.31	N/A	6.50	8.50	1.31
	62.5	14.2	22.5	9.00	12.50	1.39	94	9.00	11.00	1.22
	62.5	14.1	20.0	6.00	9.00	1.50	99	8.00	10.00	1.25
	62.8	16.7	18.8	7.50	11.00	1.47	51	7.50	9.00	1.20
	62.8	16.8	21.3	9.00	11.00	1.22	113	8.50	10.00	1.18
	62.5	18.4	20.0	8.00	11.00	1.38	101	8.00	8.50	1.06
	63.1	19.2	30.0	12.00	13.50	1.13	101	12.00	12.50	1.04
	62.6	20.0	27.5	10.00	13.00	1.30	150	11.00	12.00	1.09
	63.6	20.1	22.5	9.00	12.00	1.33	111	9.00	11.00	1.22
	64.8	19.8	22.5	9.00	12.00	1.33	109	9.00	11.00	1.22
	65.9	18.4	31.3	11.00	15.50	1.41	99	12.50	14.50	1.16
	66.6	7.9	21.3	8.50	13.00	1.53	100	8.50	10.50	1.24
	68.3	11.8	28.8	11.00	14.00	1.27	99	11.50	13.00	1.13
	69.2	8.2	23.8	11.00	15.00	1.36	41	9.50	11.00	1.16
Means			20.7			1.30	96			1.17
	X	Y	size (μm)	X l_o	X l_f	X stretch				
TA28-y-1	43.0	11.9	157.5	63.00	82.00	1.30				
	51.9	14.0	21.3	8.50	11.00	1.29				
Means			89.4			1.30				
	X	Y	size (μm)	X l_o	X l_f	X stretch				
TA28-y-2	57.6	17.3	10.0	4.00	6.00	1.50				
	X	Y	size (μm)	X l_o	X l_f	X stretch				
TA28-y-3	39.2	11.5	7.5	3.00	5.00	1.67				
	X	Y	size (μm)	X l_o	X l_f	X stretch				
TA28-y-4	42.9	12.4	12.5	5.00	8.00	1.60				
	46.3	17.0	195.0	78.00	100.00	1.28				
	45.3	12.0	7.5	3.00	4.00	1.33				
	47.0	9.1	7.5	3.00	4.00	1.33				
	64.5	10.0	12.5	5.00	7.00	1.40				
	67.5	11.0	10.0	4.00	5.50	1.38				
Means			40.8			1.39				
	X	Y	size (μm)	X l_o	X l_f	X stretch				
TA28-y-6	46.3	16.8	47.5	19.00	23.50	1.24				
	X	Y	size (μm)	X l_o	X l_f	X stretch				
TA28-y-7	44.4	13.6	17.5	7.00	9.50	1.36				
	47.7	15.5	10.0	4.00	6.00	1.50				
	50.4	14.5	32.5	13.00	17.00	1.31				
	61.0	14.4	32.5	8.00	11.00	1.38				
	64.0	11.6	125.0	50.00	65.00	1.30				
	64.4	15.4	22.5	9.00	11.50	1.28				
	68.6	15.6	15.0	6.00	8.00	1.33				

Means			36.4			1.35				
HM17	X	Y	size (μm)	X l_o	X l_f	X stretch	Rake X	Y l_o	Y l_f	Y stretch
HM17-z-1	39.9	12.4	7.5	3.00	5.00	1.67	79	3.00	3.00	1.00
	40.0	15.4	12.5	5.00	6.50	1.30	92	5.00	5.00	1.00
	44.5	15.8	45.0	9.00	18.00	2.00	79	34.00	34.00	1.00
	46.5	23.2	11.3	5.00	7.00	1.40	95	4.50	4.50	1.00
	46.9	18.1	12.5	5.00	7.00	1.40	71	5.00	5.50	1.10
	54.6	14.3	15.0	5.00	7.50	1.50	94	6.00	6.00	1.00
	49.7	22.9	12.5	5.00	7.50	1.50	87	5.00	5.50	1.10
	49.9	23.1	12.5	4.00	6.00	1.50	106	5.00	5.00	1.00
	49.7	22.9	8.8	4.00	5.75	1.44	96	3.50	3.50	1.00
	49.7	22.8	10.0	3.50	5.50	1.57	80	4.00	4.50	1.13
Means			14.8			1.53	88			1.03
	X	Y	size (μm)	X l_o	X l_f	X stretch	Rake X	Y l_o	Y l_f	Y stretch
HM17-z-2	40.8	13.7	12.5	5.00	8.00	1.60	83	5.00	5.00	1.00
	42.7	16.1	12.5	4.50	6.50	1.44	76	5.00	5.00	1.00
	43.9	17.0	12.5	5.00	8.00	1.60	79	5.00	5.00	1.00
	47.5	22.0	12.5	5.00	8.00	1.60	85	5.00	5.00	1.00
	49.6	21.7	13.8	6.00	8.50	1.42	78	5.50	5.50	1.00
	49.0	20.9	8.8	3.50	6.00	1.71	81	3.50	3.50	1.00
	48.8	20.5	10.0	4.00	6.00	1.50	80	4.00	4.00	1.00
	50.4	21.9	8.8	4.50	6.50	1.44	81	3.50	3.50	1.00
	51.1	22.4	17.5	7.00	10.00	1.43	82	7.00	7.00	1.00
	50.6	21.8	10.0	4.00	6.50	1.63	86	4.00	4.00	1.00
	49.8	17.4	12.5	5.00	7.00	1.40	83	5.00	5.00	1.00
	46.8	15.4	10.0	4.00	6.75	1.69	93	4.00	4.00	1.00
	53.3	21.1	15.0	6.00	9.50	1.58	89	6.00	6.00	1.00
	49.5	11.3	17.5	7.50	10.00	1.33	75	7.00	8.00	1.14
	66.3	22.0	15.0	6.00	9.00	1.50	82	6.00	6.00	1.00
	65.5	21.4	20.0	7.00	11.00	1.57	80	8.00	8.00	1.00
Means			13.0			1.53	82			1.01
	X	Y	size (μm)	X l_o	X l_f	X stretch				
HM17-y-2	47.0	11.9	7.5	3.00	5.00	1.67				
	48.5	11.5	12.5	5.00	7.00	1.40				
	50.0	14.3	6.3	2.50	4.00	1.60				
	51.9	12.5	15.0	6.00	10.50	1.75				
	56.1	12.9	8.8	3.50	5.50	1.57				
	60.7	14.0	12.5	5.00	7.50	1.50				
	62.2	15.0	16.3	6.50	10.00	1.54				
	63.0	17.0	13.8	5.50	9.00	1.64				
	63.3	14.4	13.8	5.50	9.00	1.64				
	63.8	14.6	25.0	10.00	16.00	1.60				
	65.3	15.0	12.5	5.00	7.00	1.40				
Means			13.1			1.57				